

Space Weather



RESEARCH ARTICLE

10.1029/2020SW002579

Special Section:

Scientific Challenges of Space Weather Forecasting Including Extremes

Extreme-Event Magnetic Storm Probabilities Derived From Rank Statistics of Historical Dst Intensities for Solar Cycles 14–24

Jeffrey J. Love¹ 

¹U.S. Geological Survey Geomagnetism Program, Denver, CO, USA

Key Points:

- Magnetic-storm-maximum $-Dst_m$, ranked per solar cycle, are well represented by a Weibull model
- Based on geomagnetic data for solar cycles 14–24 yields, a 100-year storm has an intensity of at least $-Dst_m = 663$ nT
- Based on geomagnetic data for solar cycles 14–24, the average return rate for a storm as intense as March 1989 ($-Dst_m = 565$ nT) is less than 4.1 solar cycles

Supporting Information:

Supporting Information may be found in the online version of this article.

Correspondence to:

J. J. Love,
jlove@usgs.gov

Citation:

Love, J. J. (2021). Extreme-event magnetic storm probabilities derived from rank statistics of historical Dst intensities for solar cycles 14–24. *Space Weather*, 19, e2020SW002579. <https://doi.org/10.1029/2020SW002579>

Received 30 JUN 2020

Accepted 27 FEB 2021

Abstract A compilation is made of the largest and second-largest magnetic-storm-maximum intensities, $-Dst_1$ and $-Dst_2$, for solar cycles 14–24 (1902–2016) by sampling Oulu Dcx for cycles 19–24, using published $-Dst_m$ values for 4 intense storms in cycles 14, 15, and 18 (1903, 1909, 1921, 1946), and calculating 15 new storm-maximum $-Dst_m$ values (reported here) for cycles 14–18. Three different models are fitted to the cycle-ranked $-Dst_1$ and $-Dst_2$ values using a maximum-likelihood algorithm: A Gumbel model, an unconstrained Generalized-Extreme-Value model, and a Weibull model constrained to have a physically justified maximum storm intensity of $-Dst_m = 2500$ nT. All three models are good descriptions of the data. Since the best model is not clearly revealed with standard statistical tests, inference is precluded of the source process giving rise to storm-maximum $-Dst_m$ values. Of the three candidate models, the constrained Weibull gives the lowest superstorm occurrence probabilities. Using the compiled data and the constrained Weibull model, a once-per-century storm intensity is estimated to be $-Dst_1 = 663$ nT, with a bootstrap 68% confidence interval of [497, 694] nT. Similarly, the probability that a future storm will have an intensity exceeding that of the March 1989 superstorm, $-Dst_m > 565$ nT, is 0.246 per cycle with a 68% confidence interval of [0.140, 0.311] per cycle. Noting (possibly slight) ambiguity in the rankings of storm intensities, using the same methods, but storms more intense than those identified for cycles 14–16, would yield a higher once-per-century intensity and a higher probability for a $-Dst_m > 565$ nT storm.

Plain Language Summary Past and possible future magnetic storm intensities are investigated. As part of this work, a dataset is developed of the most intense and second most intense storms for each of the past 11 solar cycles (1902–2016)—augmenting a traditional dataset that only covers the past 6 solar cycles (1957–2016) with recently published intensities for several magnetic superstorms and with new storm intensity estimates, reported here and derived from historical magnetic observatory records. These data are analyzed using statistical methods that provide estimates of the probability of future magnetic superstorms. A storm as intense as that of March 1989, which caused widespread disruption of technological systems and an electricity blackout in Québec, Canada, is predicted to occur, on average, about every four solar cycles. This is twice as often as estimated using only the traditional shorter dataset. A once-per-century storm is estimated to be substantially more intense than that of March 1989.

1. Introduction

Intense magnetic storms are hazardous for technological operations and infrastructure (e.g., Cannon et al., 2013; Daglis, 2005; Thomson, 2007). The magnetic storm of March 1989, for example, caused the collapse of the Canadian Hydro-Québec electricity transmission grid (Bolduc, 2002), caused numerous operational “anomalies” in United States power-grid systems (North American Electric Reliability Corporation, 1990), and damaged a high-voltage transformer at a nuclear power plant in Salem, New Jersey (Barnes et al., 1991; Rossi, 1990). The same storm damaged satellites and interfered with satellite operations, and it disrupted over-the-horizon radio communication and geophysical surveys around the world (e.g., Allen et al., 1989; Boteler, 2019). The magnetic storm of May 1921 caused widespread disruption to radio communication and telegraph and telephone systems (e.g., Hapgood, 2019; Silverman, 2001), and, notably, it caused fires in telegraph stations used by railroad companies in New York City and State (e.g., Love et al., 2019a). The magnetic storm of September 1909 (e.g., Hayakawa, Ebihara, Cliver, et al., 2019; Love

Published 2021. This article is a U.S. Government work and is in the public domain in the USA.

This is an open access article under the terms of the [Creative Commons Attribution License](https://creativecommons.org/licenses/by/4.0/), which permits use, distribution and reproduction in any medium, provided the original work is properly cited.

et al., 2019a; Silverman, 1995) brought interference to telegraph systems, as did the storm of October 1903 (e.g., Hayakawa, Ribeiro, et al., 2020; Ribeiro et al., 2016) and the Carrington event of September 1859 (e.g., Boteler, 2006; Green et al., 2006).

A standard measure of storm-time geomagnetic disturbance is *Dst*, a scalar time series index formed by averaging geomagnetic variation recorded at low-latitude, ground-based observatories (e.g., Mayaud, 1980; Menvielle et al., 2011). *Dst* is often interpreted in terms of the westward-directed magnetospheric ring current (e.g., Daglis, 2006). The intensification of this current during main-phase development of a magnetic storm causes a decrease in low-latitude, horizontal-component geomagnetic field strength, and, correspondingly, a decrease in *Dst* from its prestorm, near-zero value (e.g., Loewe & Prölss, 1997). This decrease in *Dst* is sometimes taken as the definition of a magnetic storm (e.g., Gonzalez et al., 1994). Storm-maximum $-Dst_m$ intensity values sampled from long durations of *Dst* are often used in statistical analyses of storm-occurrence rates (e.g., Love, 2020; Riley, 2018; Tsubouchi & Omura, 2007; Yermolaev et al., 2013). The greatest $-Dst_m$ values represent the most intense storms. These are usually driven by interplanetary coronal-mass ejections (CMEs) (e.g., Gonzalez et al., 2011; Richardson & Cane, 2012) originating from solar active regions and coronal filaments (e.g., Gopalswamy et al., 2010; Kilpua et al., 2017; Webb & Howard, 1994). The occurrence probability of intense storms waxes and wanes in broad correlation with solar-cycle increases and decreases in sunspot number (e.g., Chapman et al., 2020; Echer et al., 2011; Le et al., 2012), though the intensity and detailed evolution of each magnetic storm depend, ultimately, on the geoeffectiveness of solar-wind coupling with the Earth's magnetosphere (e.g., Lyon, 2000; Zhang et al., 2004).

While recognizing that *Dst* describes only part of each storm's complex evolution (e.g., Borovsky & Shprits, 2017; Kamide, 2006; Lanzerotti, 1992), we note that it is often used in projects for estimating space-weather hazards. This can be understood in terms of the storm-substorm relationship (e.g., Daglis et al., 2003; Kamide et al., 1998). With main-phase intensification of the magnetospheric ring current, as approximately measured by *Dst*, the auroral oval widens and slips to lower latitudes (e.g., Milan et al., 2009; Siscoe, 1976b; Yokoyama et al., 1998). Then, with the diversion of substorm currents along field lines from the ring current, through the ionosphere, and back out to the ring current (e.g., Ganushkina et al., 2017; Welling, 2019), geoelectric fields are induced in the solid Earth across mid-latitudes. Consequently, *Dst* plays an important role, though not a singular role, in projects for estimating magnetic storm hazards for electric power grids (e.g., Lucas et al., 2020; Ngwira et al., 2013; Oughton et al., 2017; Pulkkinen et al., 2012; Woodroffe et al., 2016). Thermospheric density, which affects drag on low-orbiting satellites, and spacecraft charging, which can damage onboard electronics, are observed to be correlated with intensification of $-Dst$ (e.g., Bowman et al., 2008; Ganushkina et al., 2017; Guo et al., 2010; Oliveira & Zesta, 2019) and mid-latitude geomagnetic disturbance (e.g., Koskinen et al., 2010; Qian & Solomon, 2012). Disturbances of the ionosphere, the source of storm time interference to over-the-horizon radio communication and global-positioning systems (GPS), are correlated with abrupt changes in *Dst* (e.g., Astafyeva et al., 2014; Basu et al., 2010).

In light of the history of the impacts of space weather, some scenarios anticipate that future magnetic "superstorms," often defined in terms of extreme values of *Dst* (e.g., Cliver & Dietrich, 2013; Gonzalez et al., 2011; Lakhina & Tsurutani, 2018), could bring widespread interference and damage to technological systems (e.g., Kappenman, 2012; Riley et al., 2018) and carry significant economic cost (e.g., Baker et al., 2008; Eastwood et al., 2017; Schulte in den Bäumen et al., 2014). For this reason, national and international space-weather projects (e.g., National Science and Technology Council, 2019; Schrijver et al., 2015) have identified prediction and long-term forecasting of intense storms as priorities for scientific investigation (e.g., Baker, 2002; Hapgood, 2011; Morley, 2020). In this context, we assemble and develop a dataset of storm-maximum intensities $-Dst_m$ for solar cycles 14–24 (1902–2016). We model the statistics of the most intense and second most intense storms per solar cycle using the mathematical formalism of extreme-value theory for ranked data. We examine possible secular change in the data and possible correlations of the $-Dst_m$ values with sunspot number. We estimate future storm occurrence probabilities and associated confidence intervals. Results inform projects for improving societal resilience to space-weather hazards (e.g., Green et al., 2016; Jonas et al., 2016).

2. Observatory Data

The foundation of our analysis is historical geomagnetic variation data collected at ground-based observatories (e.g., Love, 2008; Rasson et al., 2010). Since the 1980s, most of these observatories, including those considered here, have operated electronic fluxgate magnetometers and digital acquisition systems (e.g., Jankowski & Sucksdorff, 1996; Newitt, 2007). The standard products of these observatories are 1-min and (more recently) 1-s resolution time series. These data have a wide variety of applications, including for monitoring variable space-weather conditions, hazard evaluation, studies of the solid Earth, and geomagnetic modeling and mapping (e.g., Kerridge, 2001; Love & Chulliat, 2013). Before the 1980s and since the mid-19th century, magnetic observatory monitoring relied on analog variometer systems (e.g., Schröder & Wiederkehr, 2000). For each geomagnetic vector component, a beam of light was projected onto a tiny mirror attached to a freely orienting magnetized needle. As the geomagnetic field varied in time, the light beam was deflected back and forth, and this was recorded on a photographic paper mounted onto a cylinder that rotated once per 24 h. Each day, the paper was removed from the cylinder, and, when it was developed, the light trace provided a time-series magnetogram. Depending on the convention of the observatory institute, hourly spot values or hourly average values were measured using a gauge (expressed, e.g., in mm). Magnetic units were obtained by applying conversion factors (e.g., nT/mm). For many years, it was traditional to report hourly data in published yearbooks, often along with reproductions of magnetograms for major storms. These days, hourly values, and other data resolutions, are reported to the World Data System (WDS).

3. Kyoto and Oulu Versions of *Dst*

The *Dst* index was developed during the International Geophysical Year (IGY 1957–1958) (Sugiura, 2006; Sugiura & Kamei, 1991), when observatory operations around the world were improved and harmonized (e.g., Various, 1957). Today, the calculation of the standard version of *Dst* is a service provided by World Data Center for Geomagnetism, Kyoto et al. (2015) (WDC); the index covers years 1957–2016 (most of solar cycle 19 to cycle 24). In summary, sequential 1-h data values recording horizontal component geomagnetic field variation are obtained from four long-running, low-latitude, ground-based observatories that are widely separated in longitude: Hermanus (HER), South African National Space Agency (e.g., Kotzé, 2018), Kakioka (KAK), Japan Meteorological Agency (e.g., Minamoto, 2013), Honolulu (HON) and San Juan (SJG), U.S. Geological Survey (USGS) (e.g., Love & Finn, 2011). For 1957–2016, these hourly values are boxcar hour averages centered at the bottom of the universal-time (UT) hour (00:30, 01:30, etc.). A nonstormy, quiet-time baseline is subtracted from each observatory time series; *Dst* is a weighted average of the residual disturbance time series from the four observatories. Each Kyoto hourly *Dst* value is centered and timestamped on the bottom of the UT hour. Although widely used in the space-physics and space-weather communities, we recognize that Kyoto *Dst* is calculated using an odd normalization of the data streams from the four source observatories (e.g., Love & Gannon, 2009, Section 4).

Using digital files of historical hourly observatory data from the WDS, Karinen and Mursula (2005) of Oulu University, Finland have reconstructed *Dst* using a corrected data normalization (Mursula et al., 2008). This index is sometimes known as *Dcx*. It is available in different versions, including a four-observatory version for 1957–2016 that is calculated using the same source observatory data used to calculate Kyoto *Dst*; other versions of the Oulu *Dst* index are calculated using data from additional low-latitude observatories, up to 17 for some years. Due to differences in normalization, at storm maximum, the average relative difference, $|Dst_m^{Kyoto} - Dst_m^{Oulu}| / |Dst_m^{Oulu}|$ (for four-station versions of the indices) is about 3%. Since the many-observatory versions of Oulu *Dst* involve a lot more geographic averaging than a four-observatory *Dst*, the many-observatory version is less affected by localized differences in geomagnetic disturbance. In this respect, the many-observatory version of the index is more accurate than a four-station *Dst*. At storm maximum, the average relative difference between the Oulu four-observatory and multiobservatory versions is about 8%. Mindful of these issues, in our statistical analysis of storm intensities, for cycles 19–24 (1957–2016), we use the Oulu corrected storm-maximum $-Dst_m$ values, and, when available, we use the multiobservatory version of Oulu $-Dst_m$, Section 5; we do not use Kyoto *Dst*.

Estimating *Dst* for years prior to IGY (before 1957) can be challenging due to different and changing data-reporting conventions and the geographic sparsity of observatories. We have two related quibbles that affect the quality of the pre-IGY extension of the four-observatory version of the Oulu *Dst* index back to 1932, which is calculated using data from Cape Town (CTO) South Africa, KAK, HON, and SJG. The first concerns timestamp conventions. Before and including 1956, for example, KAK observatory data are reported in yearbooks as spot values with timestamps at the top of each UT hour (00:00, 01:00, etc.) (Kakioka Magnetic Observatory, 1959, p. 9); on the other hand, the pre-IGY HON and SJG data (all the way back to 1915) follow the post-IGY convention of hourly averages centered on the bottom of the UT hour (e.g., Hazard, 1918, p. 5); the same is true for all of the CTO data back to 1932 (e.g. Magnetic Observatory, University of Cape Town, 1944). These important issues are not recorded in the digital files held by the WDS, but they can make a difference when averaging the data to calculate *Dst*—for given HON, SJG, and CTO data (from, say, 00:30 UT), which KAK data value should be used (00:00 or 01:00) in an average? Linear interpolation of the KAK data to obtain values at the bottom of the hour results in degraded 2-h resolution. We do not know how the KAK timestamp is handled for pre-IGY Oulu *Dst*. Our second quibble concerns the reporting of data gaps. For some magnetic storms, observatory hourly values are fillers intended to indicate that either the light trace of the analog magnetometer system had wandered off the edge of the photographic paper (as we discuss in Section 2, during periods of great geomagnetic disturbance), or, for whatever reason, an hourly value was difficult to estimate. Filler values should be treated as data gaps; they should not be used in calculating *Dst*. The presence of fillers is indicated in observatory yearbooks (such as with footnotes or other notations), but this important information is not given in the WDS files. A difficult example of this is seen with the HON data for the July 1941 storm, three hourly values are fillers. Unfortunately, the 1941 HON yearbook, held in National Oceanic and Atmospheric Administration archives in Boulder, Colorado, was never formally published (likely due to priorities brought by the World War); a photograph of the relevant yearbook page for HON July 1941 is given in a supplementary file accompanying this report. Inspection of the HON July 1941 time series on the Oulu website shows that filler values are not properly treated in the calculation of Oulu *Dst*. Mindful of these issues, for cycles 14–18, we use $-Dst_m$ values taken either from publications on specific storms, or we calculate $-Dst$ using data values taken from yearbooks and WDS digital files, Section 6. We show the Oulu *Dst* time series from 1932 to 2016 in Figure 1a.

4. Autocorrelation and Sampling

We adopt a statistical approach for analyzing storm-maximum intensity values and predicting future probabilities, but autocorrelation in the *Dst* time series is incompatible with the data independence that is often assumed in statistical analyses. Most obviously, the *Dst* time series is serially correlated—space-weather conditions vary continuously in time, and, as a result, from one hour to the next, a particular *Dst* value is often similar to that of the previous and subsequent hour. This applies during quiet conditions, and it applies during the one- to three-day durations of magnetic storms, though the hour-to-hour variance in *Dst* is higher during a magnetic storm than it is during quiet times. Over longer timescales, the occurrence of one storm is often correlated with the occurrence of other storms due to the nature of the solar wind (e.g., Borovsky, 2020). So, for example, a sunspot group might be the source of multiple coronal mass ejections, each causing a separate magnetic storm (e.g., Gonzalez et al., 2011), or a high-speed stream of plasma emitted from a long-lasting coronal hole can sometimes cause a pair of magnetic storms separated in time by a solar-rotation period (e.g., Richardson & Cane, 2012; Tsurutani et al., 2006).

Data suitable for statistical analysis can be extracted from a time series by down-sampling or averaging over timescales longer than those characteristic of the autocorrelations (e.g., von Storch, 1995; Wilks, 2019, Chapter 5.2.4). A simple sampling method, often used in extreme-event analysis, is selecting the maximum values from ranked sequences of data in blocks of time covering a data time series (e.g., Coles, 2001, Chapter 1.1; Davison & Huser, 2015, Section 2). Block-maximum sampling removes autocorrelation over timescales shorter than the duration of each block; it is used, in particular, in analyses of stochastic processes that are modulated periodically or quasi-periodically. So, for example, statistical analyses are made of annual-maximum rainfall (e.g., Katz et al., 2002). In our study, the natural modulation to consider is that of the solar cycle. Identification of the most intense and second most intense storms, $-Dst_1$ and $-Dst_2$, for each solar cycle, is a type of block-maximum sampling.

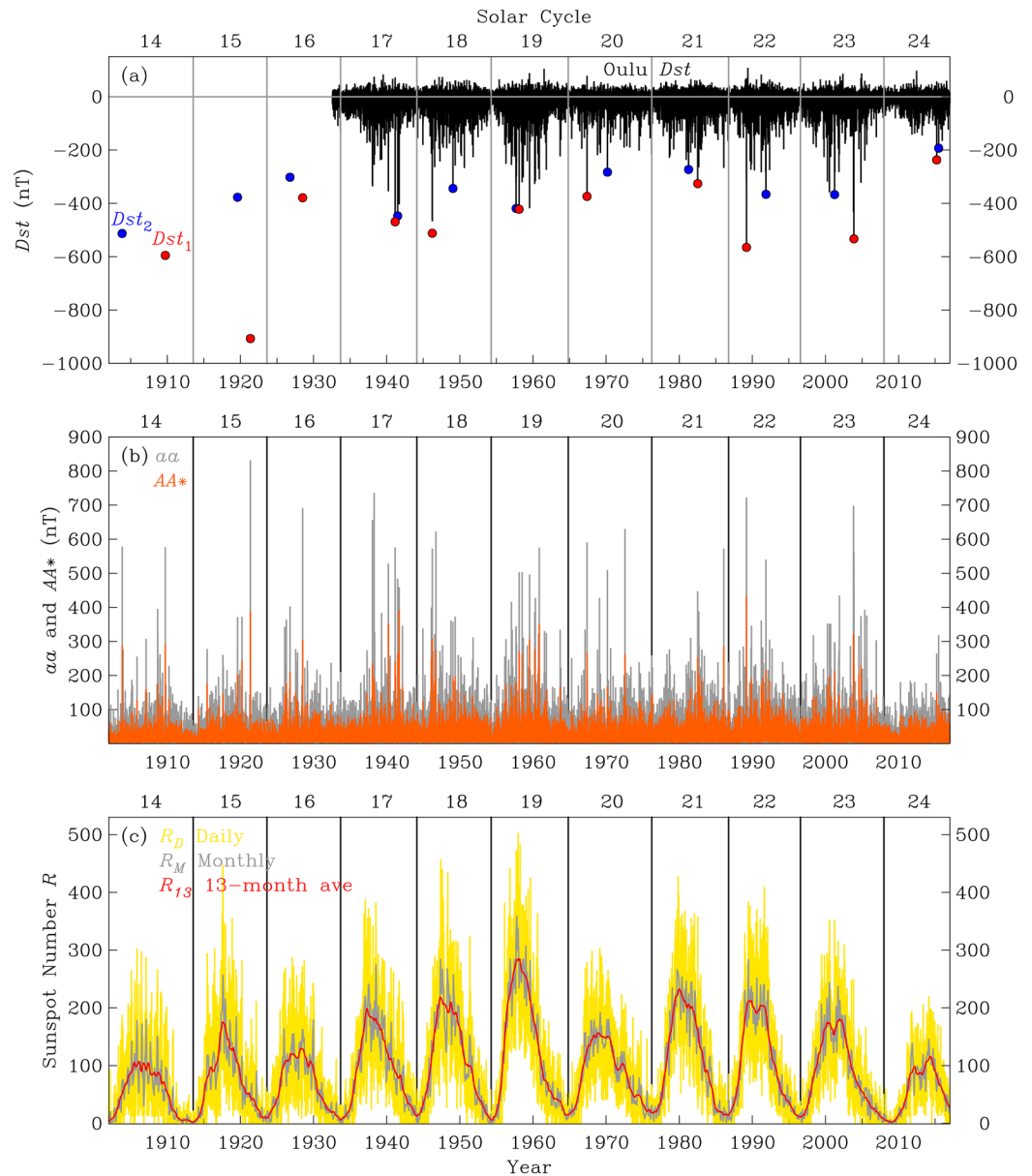


Figure 1. (a) The Oulu Dst time series (black), 1932–2016 (solar cycles 17–24) and the most intense and second most intense values, Dst_1 (red) and Dst_2 (blue), cycles 14–24, used in our statistical analysis (Table 1). (b) The aa (gray) and the 24-h running average AA^* (orange) time series. (c) Sunspot numbers, daily R_D (yellow), monthly R_M (gray), and 13-month running average R_{13} (red).

5. Storm Intensities: Solar Cycles 19–24

We rank storm-maximum $-Dst_m$ value from the Oulu Dst time series within each solar cycle, Figure 1a, keeping the most intense $-Dst_m = -Dst_1$ and second most intense $-Dst_m = -Dst_2$ storms for each of solar cycles 19 to 24 (years 1954–2016). In Table 1, we list these values. The most intense storm of cycle 19 was that of February 1958 ($-Dst_1 = 422$ nT), followed closely by that of September 1957 ($-Dst_2 = 419$ nT). For cycle 20, the most intense storm was that of May 1967 (e.g., Knipp et al., 2016; Webb, 1969) ($-Dst_1 = 374$ nT), followed by that of March 1970 (e.g., Pudovkin et al., 1972) ($-Dst_2 = 283$ nT). For cycle 21, the most intense storm was that of July 1982 ($-Dst_1 = 326$ nT) (e.g. Wik et al., 2009), followed by that of April 1981 ($-Dst_2 = 273$ nT). For cycle 22, the Québec storm of March 1989 was the most intense ($-Dst_1 = 565$ nT), indeed, this was the most intense storm since the IGY; the second most intense storm of this cycle was

Table 1
Summary of Magnetic Storm Intensities $-Dst_m$ and Related Factors

SC	Year	Month	Day	$-Dst_m$ (nT)	Rank	Observatory data used	Source	AA_m^*	Rank (nT)	R_{D-2}	R_M (nT)	R_{13}
14	1903	10	31	513	2 [†]	COI CLA ZKW CUA	Hayakawa, Ribeiro, et al., 2020	287.5	2	47	64.8	49.4
	1907	02	09	340		SFS VQS	This study	160.9	4			
	1908	09	12	280		SFS API	This study	176.8	3			
	1909	05	14	278		SFS VQS	This study	138.3	5			
	1909	09	25	595	1 [†]	SFS MRI API VQS	Love et al. (2019a)	291.7	1			
15	1915	06	17	255		SFS TUC VQS	This study	176.9	4	92	64.7	63.7
	1917	08	09	199		HON VQS	This study	145.9	5			
	1919	08	11	300		SFS HON VQS	This study	203.1	3			
	1920	03	23	377	2 [†]	SFS HON TUC	This study	243.7	2			
	1921	05	15	907	1 [†]	WAT API VSS	Love et al. (2019b)	388.4	1			
16	1926	01	26	194		SFS WAT HON SJG	This study	148.5	5	252	119.3	115.9
	1926	04	15	252		WAT HON TUC	This study	177.1	3			
	1926	10	15	302	2 [†]	SFS WAT HON TUC	This study	209.7	2			
	1927	07	22	200		WAT TUC	This study	151.3	4			
	1928	07	08	379	1 [†]	SFS WAT HON TUC	This study	304.3	1			
17	1941	03	01	469	1	HER WAT API	This study	240.0	4	83	77.5	88.0
	1941	07	05	447	2	HER WAT TUC SJG	This study	264.5	3			
18	1946	03	28	512	1	COI CLA ZKW CUA	Hayakawa, Ebihara, et al., 2020	309.8	1	95	127.7	121.5
	1949	01	26	344	2	HER WAT HON SJG	This study	190.8	5			
19	1957	09	13	419	2	HER KAK HON SJG	Oulu	149.6	17	347	334.0	279.3
	1958	02	11	422	1	HER KAK HON SJG	Oulu	271.5	4			
20	1967	05	26	374	1	HER KAK HON SJG	Oulu	266.2	1	225	122.5	123.9
	1970	03	08	283	2	HER KAK HON SJG	Oulu	167.8	3			
21	1981	04	13	273	2	HER KAK SJG	Oulu	129.2	11	288	225.3	205.7
	1982	07	14	326	1	HER KAK HON SJG	Oulu	252.9	2			
22	1989	03	14	565	1	HER KAK HON	Oulu	433.2	1	182	170.4	203.8
	1991	11	09	366	2	HER KAK HON SJG	Oulu	217.6	2			
23	2001	03	31	367	2	17 Observatories	Oulu	214.4	4	340	165.8	155.1
	2003	11	20	533	1	17 Observatories	Oulu	233.8	2			
24	2015	03	17	237	1	14 Observatories	Oulu	149.7	1	53	54.5	82.1
	2015	06	23	193	2	14 Observatories	Oulu	116.0	3			

Note: The most intense (Rank 1, $-Dst_1$) and second most intense (Rank 2, $-Dst_2$) storm intensities, for each of solar cycles (SC) 14 to 24 (years 1902–2016); inferred storm-intensity ranks are denoted with †. Oulu and previously published intensities (as noted) and new intensity estimates (this study) are derived from magnetic observatory data: Apia (API), Coimbra (COI), Colaba (CLA), Cuajimalpa (CUA), Hermanus (HER), Honolulu (HON), Kakioka (KAK), Mauritius (MRI), San Fernando (SFS), San Juan (SJG), Tucson (TUC), Vieques (VQS), Vassouras (VSS), Watheroo (WAT), Zi-Ka-Wei (ZKW). Also listed are AA_m^* and their solar-cycle ranks, and sunspot number averages, R_{D-2} , R_M , R_{13} .

that of November 1991 ($-Dst_2 = 366$ nT). For cycle 23, the most intense storm was that of November 2003 ($-Dst_1 = 533$ nT), which came after the more vigorous, but in terms of maximum $-Dst_m$, slightly smaller Halloween storm of October 2003 (e.g., Balch et al., 2004; Gopalswamy et al., 2005); the second most intense storm of this cycle was that of March 2001 ($-Dst_2 = 367$ nT). Cycle 24 was notably weak; the St. Patrick's day storm of March 2015 was the most intense (e.g., Wu et al., 2016) ($-Dst_1 = 237$ nT), followed by that of June 2015 ($-Dst_2 = 193$ nT).

6. Storm Intensities: Solar Cycles 14–18

We list, in Table 1, $-Dst_m$ intensities for 19 magnetic storms that occurred in solar cycles 14 to 18 (years 1902–1954); this list helps fill in and extend back in time lists of storms given by other investigators (e.g., Bell et al., 1997; Gonzalez et al., 2011; Lakhina & Tsurutani, 2018; Vennerstrom et al., 2016). Four of these storm intensities are from published papers: October 1903 (Hayakawa, Ribeiro, et al., 2020), September 1909 (Love et al., 2019a), May 1921 (Love et al., 2019b), and March 1946 (Hayakawa, Ebihara, et al., 2020). The other 15 storm intensities are estimated using methods like those used by others for estimating pre-1957 Dst (e.g., Hayakawa, Ribeiro, et al., 2020; Love et al., 2019a,b). In summary, we inspect observatory yearbooks and WDS data files. For each storm and for each observatory record, we check timestamp conventions, and we check for data gaps and filler values. We make a point of searching for data from low-latitude observatories that are widely separated in longitude to obtain a good circum-global-average measure of storm disturbance. For various reasons, we sometimes use data from observatories that are different from those used for calculating standard versions of Dst . For example, we identify three acceptable observatory records for the March 1920 storm; noting that no observatory was operated in South Africa until 1932, we use San Fernando (SFS), Spain yearbook data (Instituto y Observatorio de Marina, 1921); we found no suitable records for Asian-Australian longitudes, we do not use any KAK data because of incompatibility of timestamps; we use HON WDS data files (Hazard, 1922a); we use TUC WDS data files (Hazard, 1922b) in place of Vieques (VQS), Puerto Rico (the predecessor observatory to SJG) data, which have a gap (Hazard, 1923). For the October 1926 and July 1928 storms, we use Watheroo (WAT), Australia, WDS data files (Fleming et al., 1947). For the March 1941 storm, we use Apia (API), Samoa, WDS data files in place of HON data, which have a gap; we found no suitable records for American longitudes. For the July 1941 storm, in place of HON data, which have filler values (per yearbook), we use WDS TUC data files. For each observatory record, we subtract a pre-storm 24-h quiet period from the storm-time period to obtain disturbance data values. With latitude factors, we average the disturbance data to obtain estimates of storm-maximum $-Dst_m$.

We examine the validity of our identification of $-Dst_1$ and $-Dst_2$ for solar cycles 17 and 18 by comparing them with the Oulu Dst index. Our cycle-ranked $-Dst_1$ and $-Dst_2$ data values and that of Hayakawa, Ebihara, et al. (2020) for the March 1946 storm, Table 1, are all slightly greater than the corresponding Oulu $-Dst_1$ and $-Dst_2$ values. The average relative difference is 5%. This is less than the 8% averaging error we estimate for Dst_1 and Dst_2 in Section 3. Therefore, even though we have some quibbles with parts of the Oulu Dst time series, Section 3, we understand that the Oulu Dst time series is accurate enough to allow us to confidently identify which storms are the most intense and second most intense, $-Dst_1$ and $-Dst_2$, for cycles 17 and 18. For cycle 17, the storm of March 1941 (e.g., Parkinson, 1941; White, 1941) was the most intense ($-Dst_1 = 469$ nT), and the storm of July 1941 (e.g., Nelson, 1941; Ogg, 1941) was the second most intense ($-Dst_2 = 447$ nT). For cycle 18, the storm of March 1946 (e.g., Ogg, 1946; Parkinson, 1946) was the most intense ($-Dst_1 = 512$ nT), and the storm of January 1949 was the second most intense ($-Dst_2 = 344$ nT).

Lacking a time-continuous record of Dst for earlier solar cycles, we seek an objective method for identifying each cycle's most intense storms. We turn to the aa index, a mid-latitude measure of the range of geomagnetic vector variation over 3-h windows of time at two nearly antipodal observatories (one in the northern hemisphere and one in the southern hemisphere) (Mayaud, 1980). The aa index is continuous in time from 1868 to the present, and so it covers our period of interest. Extended durations of high aa represent vigorous magnetospheric convection (e.g., Thomsen, 2004) leading up to storm-maximum intensity as measured by $-Dst_m$ (e.g., Ebihara & Ejiri, 1998; Jordanova et al., 2001). Therefore, using a “homogeneous” version of aa (Lockwood, Chambodut, et al., 2018), Figure 1b, we calculate a running 24-h average of the index time series, something often called AA^* . In Table 1, the listed storms for each of cycles 14–16 have the highest-ranked maximum values $AA_m^* = AA_1^*, \dots, AA_5^*$, and, from calculated $-Dst_m$ for each of those storms, we infer each cycle's $-Dst_1$ and $-Dst_2$. For example, we infer that the most intense and second most intense storms of cycle 14 were, respectively, those of September 1909 ($-Dst_1 = 595$ nT) and October 1903 ($-Dst_2 = 513$ nT); we note that those two storms exhibited the cycle's highest AA_1^* and second-highest AA_2^* levels of mid-latitude disturbance. The intensities of three other storms, and notably that of February 1907 ($-Dst_m = 340$ nT), do not exceed that of October 1903. We infer that the most intense and second most intense storms of cycle 15 were those of May 1921 (e.g., Angenheister & Westland, 1921; Parkinson, 1921) ($-Dst_1 = 907$ nT) and March 1920 (e.g., Faris, 1920; Hazard, 1920) ($-Dst_2 = 377$ nT); for cycle 16, we infer they were the storms of July

1928 (e.g., Johnston, 1928) ($-Dst_1 = 396$ nT) and October 1926 (e.g., Johnston, 1927) ($-Dst_2 = 302$ nT). In each case, those storms also exhibited their cycle's highest AA_1^* and second-highest AA_2^* levels of mid-latitude disturbance.

Though we identify intense storms, there is room for doubt as to whether or not our identification of $-Dst_1$ and $-Dst_2$ are, in fact, the most intense and second most intense storms of solar cycles 14–16. We would like to estimate the confidence we can have in our inferred rankings. We note from Table 1 that, for six of the eight of cycles 17–24, the $-Dst_1$ and $-Dst_2$ values are among the storms with the five highest AA_m^* ; for cycle 19, $-Dst_2$ is associated with the 17th highest AA_m^* , and for cycle 21, $-Dst_2$ is associated with the 11th highest AA_m^* . We might, therefore, estimate that the probability that the correct $-Dst_1$ and $-Dst_2$ are among the storms with the five highest AA_m^* for any particular solar cycle is $6/8$ or 0.750 . From this, the joint probability that storms with the five highest AA_m^* for all three of cycles 14–16 will be $-Dst_1$ and $-Dst_2$ for each cycle is $(0.750)^3 = 0.422$. In other words, under the assumptions made here, there might be a reasonably large probability (0.578) that the correct $-Dst_1$ and $-Dst_2$ for cycles 14–16 are greater than those we identify. Despite this, we suspect that we have, in fact, identified the most intense storms for these cycles, but because of lingering uncertainty, we regard the $-Dst_1$ and $-Dst_2$ intensities listed in Table 1 for solar cycles 14–16 as lower bounds on storm intensities for those cycles. This affects our choice of model in Section 12.

7. Secular Change

Qualitatively, the solar-cycle-ranked storm intensities, $-Dst_1$ and $-Dst_2$, shown in Figure 1a and listed in Table 1, are not uniformly distributed in time. There were, for example, four so-called superstorms, with $-Dst_m > 500$ nT (e.g., Lakhina & Tsurutani, 2018), during solar cycles 14–18 (October 1903, September 1909, May 1921, March 1946), but only two such storms occurred during cycles 19–24 (March 1989 and November 2003). Considering, first, the most intense storms of each cycle, a Kolmogorov-Smirnov test (e.g., Bohm & Zech, 2010, Chapter 10.3.5; Press et al., 1992, Chapter 14.3) indicates that the discrepancies between the distributions of the $-Dst_1$ intensities for cycles 14–18 and for cycles 19–24 are something that would be exceeded by random data with a probability of $p = 0.367$. For the second most intense storms of each cycle, $-Dst_2$, $p = 0.367$, the same value as for $-Dst_1$ due to small data numbers. These probabilities are of marginal significance, insufficient to comfortably dismiss the possibility that the discrepancies are only due to random fluctuations in data taken from the same distribution. Still, if any of the estimates of $-Dst_1$ or $-Dst_2$ for cycles 14–16 are underestimates, a possibility we discuss in Section 6, then we might have statistically significant evidence of secular change in storm intensities; but, for now, we do not have such evidence.

For data, such as $-Dst_1$ and $-Dst_2$, that are positive with possible outliers, it is useful to analyze the statistics of their logarithms (e.g., Tukey, 1977). The geometric mean, which for a set of n positive data $\{x^i\}$ is

$$m = \exp \left[\frac{1}{n} \sum_{i=1}^n \ln(x^i) \right]. \quad (1)$$

If we accept the cycle rankings given in Table 1 as they are, then, the geometric mean of $-Dst_1$ for cycles 14–24 is 457 nT; and this appears to be a relatively well-centered mean; out of 11 cycles, 6 had $-Dst_1 > 457$ nT and 5 $-Dst_1 < 457$ nT. For cycles 14–18, the geometric mean of $-Dst_1$ is 547 nT, but for cycles 19–24, it is much lower at 393 nT. Student's t test (e.g., Bohm & Zech, 2010, Chapter 3.6.11; Press et al., 1992, Chapter 6.2) gives $p = 0.125$ that the means for cycles 14–18 and cycles 19–24 would arise from two distributions with the same mean. The geometric mean of $-Dst_2$ for cycles 14–18 is 390 nT, but for cycles 19–24, it is lower at 307 nT; Student's t test gives $p = 0.153$. As with the Kolmogorov-Smirnov tests, these probabilities, for the geometric means of either $-Dst_1$ or $-Dst_2$, are of marginal significance, insufficient to comfortably dismiss the possibility that it is only a statistical fluke that storms were more intense during cycles 14–18 than during cycles 19–24. Again, the data do not provide persuasive statistical evidence of a long-term systematic change (over the past 11 solar cycles) in storm intensity.

A related issue is possible correlation between cycle-maximum storm intensity $-Dst_1$ and sunspot number. As we already noted, and as is well known, the probability of intense storms is modulated roughly in correlation with the rise and decline in sunspot number with each solar cycle, though there are excep-

tions to this rule—notably, the storm of October 1903 came very early in cycle 14 (e.g., Hayakawa, Ribeiro, et al., 2020). However, our interest here is not the details of intra-cycle modulation but, rather, a possible long-term relationship between cycle-maximum storm intensity and sunspot number. In Figure 1c, we plot daily R_D , monthly average R_M , and 13-month running average R_{13} sunspot number for solar cycles 14–24 (Clette et al., 2014; SILSO World Data Center, 1902–2016). In Table 1, we list sunspot number R_{D-2} for 2 days before each $-Dst_m$, and we list R_M and R_{13} , for each $-Dst_m$. We calculate the Pearson correlation coefficient (e.g., Press et al., 1992, Chapter 14.5) between these sunspot numbers and $-Dst_1$. For R_{D-2} , the correlation is small and, possibly surprisingly, negative, -0.154 , but the probability that such a correlation coefficient could be realized from random data, is large, $p = 0.651$. For R_M (R_{13}) and $-Dst_1$, the correlation coefficient is -0.352 (-0.360), and $p = 0.288$ ($p = 0.275$). None of these correlations can be deemed significant.

A similar insignificant correlation is found by Kilpua et al. (2015) between aa and sunspot number. They interpreted this as due to a small-scale turbulent dynamo process in the Sun, one that is only indirectly related to the generation of sunspots. Indeed, we note that energetic solar flares (and, therefore, CMEs) most frequently originate in active regions with complex heliomagnetic polarity structures (fragmentation, helicity) (e.g., Lefèvre et al., 2016; Sammis et al., 2000). CMEs can also originate in disappearing filaments, sometimes at locations in the corona rather far removed from active regions (e.g., Gopalswamy et al., 2010; Webb et al., 2000); an example of a storm generated by such a CME is that of November 1991 (e.g., Cliver et al., 2009), $-Dst_2 = 366$ nT. These several factors are not well measured by sunspot number, and, therefore, we appreciate that sunspot number is not likely to be tightly correlated with cycle-maximum magnetic storm intensity. Multiply this by the fact that the geoeffectiveness of a CME, and, therefore, storm intensity, depends on solar-wind velocity, density, and interplanetary magnetic field (IMF) strength and orientation, quantities that, themselves, evolve as the CME traverses the Sun-Earth distance. It is, therefore, unsurprising that the intensities of the most intense storms are not well correlated with sunspot number.

8. Stochastic Processes

Since our dataset of the most intense and second most intense storms, $-Dst_1$ and $-Dst_2$, for each solar cycle are ranked samples from a larger set of storm-maximum $-Dst_m$ values, in considering candidate statistical models of $-Dst_1$ and $-Dst_2$, we first consider candidate statistical models of the source $-Dst_m$ values. The most conventional model used in extreme-value statistical analyses is the power-law. For positive random data $\{x > \mu\}$ that are power-law distributed, the probability density and cumulative functions are

$$p(x, \mu, \xi) = \frac{1}{\mu^\xi} \left(\frac{x}{\mu} \right)^{-\xi-1} \quad (2)$$

and

$$P(x, \mu, \xi) = \int_{\mu}^x p(\phi, \mu) d\phi = 1 - \left(\frac{x}{\mu} \right)^{-\frac{1}{\xi}} = 1 - \bar{P}(x, \mu, \xi) \quad (3)$$

(e.g., Clauset et al., 2009; Newman, 2005; Sornette, 2006), where μ is a location parameter, ξ is a shape parameter, $\xi > 0$, and $\bar{P}(x; \mu, \xi)$ is the complementary cumulative. Some physical systems that exhibit power-law statistics can be described in terms of self-organizing criticality (SOC), whereby a system evolves to an unstable state that collapses only to evolve again to a similarly unstable state (e.g., Aschwanden, 2011; Sornette, 2006; Turcotte, 1999). In the storm-time magnetosphere, SOC is associated with the buildup of magnetic field at the magnetopause and in the magnetotail that is abruptly rearranged with reconnection (e.g., Angelopoulos et al., 1999; Chang, 1999). Power-law statistics are found in numerical simulations of substorm dynamics (e.g., Klimas et al., 2000; Uritsky & Pudovkin, 1998) and in some analyses of ground-level geomagnetic data (e.g., Balasis et al., 2009; Pulkkinen et al., 2006; Wanliss, 2005). Power-law models have been used to describe extreme-value storm intensities (e.g., Kataoka, 2013; Riley, 2012; Yermolaev et al., 2013), but the occurrence probabilities of the very most extreme intensities are often overestimated by power-law models (e.g., Riley, 2018, Figure 2).

A lognormal model is sometimes assumed to represent the statistics of storm-maximum intensities (e.g., Haines et al., 2019; Lockwood, Owens, et al., 2018; Love et al., 2015; Pulkkinen et al., 2012). For positive random data $\{x\}$ that are lognormally distributed, the probability density function is

$$l(x, \mu, \sigma) = \frac{1}{x\sqrt{2\pi\sigma^2}} \exp\left[-\frac{(\ln x - \mu)^2}{2\sigma^2}\right], \quad (4)$$

where $\ln x$ is the natural logarithm of x , and μ is the $\ln x$ -population mean, a location parameter, and σ^2 is the $\ln x$ -population variance, a scale parameter. The cumulative function is

$$L(x, \mu, \sigma) = \int_0^x l(\phi, \mu, \sigma) d\phi = \frac{1}{2} + \frac{1}{2} \operatorname{erf}\left[\frac{\ln x - \mu}{\sqrt{2}\sigma}\right] = 1 - \bar{L}(x, \mu, \sigma), \quad (5)$$

and where $\bar{L}(x; \mu, \sigma)$ is the complementary cumulative. Use of a lognormal model is often justified by appealing to the central limit theorem, under which a lognormal process arises from the multiplication of random variables generated by independent underlying processes (e.g., Crow and Shimizu, 1988; Marshall & Olkin, 2007; Mitzenmacher, 2004; Sornette, 2006). Recognizing this, we note that the solar-wind variables of velocity, density, and IMF magnetic field strength display lognormal properties (e.g., Burlaga, 2001; Burlaga & Lazarus, 2000; Veselovsky et al., 2010). It is tempting to imagine a lognormal process for storm-maximum intensities as arising from a multiplicative combination of solar-wind variables that plausibly govern the geoeffectiveness of solar-wind-magnetospheric coupling (e.g., Newell et al., 2007). However, even if spatial and temporal correlations in solar-wind variables could be removed through sampling, so as to render a statistical subset of the solar-wind data, the response of the magnetospheric-ionospheric system to solar-wind forcing is nonlinear (e.g., Vassiliadis et al., 1995), and, therefore, the statistical association of $-Dst_m$ with solar-wind variables is not straightforward.

Both the power-law and the lognormal functions asymptotically approach zero in the extreme-value limit,

$$\lim_{x \rightarrow \infty} \bar{L}(x) = 0 \quad \text{and} \quad \lim_{x \rightarrow \infty} \bar{P}(x) = 0, \quad (6)$$

but the nature of these two distributions is distinctively different as this limit is approached. The distinguishing property of the power-law distribution is its “regular-variation” or “self-similarity,” with any one part of the distribution resembling another part under rescaling by a multiplicative factor r ,

$$\frac{\bar{P}(r \cdot x)}{\bar{P}(x)} = r^{-\frac{1}{\xi}}, \quad \text{where we assume } r > 0. \quad (7)$$

On the other hand, the lognormal distribution is not regularly varying at infinity,

$$\lim_{x \rightarrow \infty} \frac{\bar{L}(r \cdot x)}{\bar{L}(x)} = \begin{cases} 0 & r \in (1, +\infty) \\ 1 & \text{for } r = 1 \\ \infty & r \in (0, 1) \end{cases}, \quad (8)$$

and the tail of the lognormal approaches zero more rapidly than that of the power law,

$$\lim_{x \rightarrow \infty} \frac{\bar{P}(x)}{\bar{L}(x)} = \infty. \quad (9)$$

In other words, for given fits to data, $\{\mu, \xi\}$ and $\{\mu, \sigma\}$, extrapolated occurrence probabilities will be higher for power-law models than for lognormal models. Although we regard these observations as important, we remain mindful of the possibility that storm statistics are not described by either power-law or lognormal processes.

We can, furthermore, consider the possibility that magnetic storm intensity has an upper limit. Ring-current intensity is likely saturated when a balance is attained between plasma pressure within the magnetosphere and the pressure of the magnetic dipole (Vasyliūnas, 2011). With such a balance, the greatest possible value for $-Dst_m$ is approximately 2500 nT, far higher than anything that has been observed. Following on from our discussion of a lognormal process, then, we might assume that magnetic storm intensities are realized from an upper-limit lognormal process (e.g. Love, 2020), where the variable $\{\ln[x / (v - x)]\}$ is normally distributed, and $\{0 < x < v\}$ is domain-right-limited, with probability density function,

$$u(x, \mu, \sigma, v) = \frac{1}{\sqrt{2\pi\sigma^2}} \frac{v}{x(v-x)} \exp\left[-\frac{(\ln[x / (v-x)] - \mu)^2}{2\sigma^2}\right]. \quad (10)$$

The corresponding cumulative function is

$$U(x, \mu, \sigma, v) = \int_0^x u(\phi, \mu, \sigma, v) d\phi = \frac{1}{2} + \frac{1}{2} \operatorname{erf}\left[\frac{\ln[x / (v-x)] - \mu}{\sqrt{2}\sigma}\right] = 1 - \bar{U}(x, \mu, \sigma, v) \quad (11)$$

(Bezdek & Solomon, 1983; Mugele & Evans, 1951). An interesting comparison is of the upper-limit lognormal distribution with a scaled beta distribution, for which the probability density function is

$$b(x, \mu, \alpha, \beta, v) = \frac{x^{\alpha-1}(v-x)\beta^{-1}}{\mathbb{B}(\alpha, \beta)v^{\alpha+\beta-1}} \quad (12)$$

(e.g. Johnson et al., 1995, Chapter 21), where $\mathbb{B}(\alpha, \beta)$ is the beta function (e.g. Spanier & Oldham, 1987, Chapter 58), and where $\alpha, \beta > 0$. The corresponding cumulative function is

$$B(x, \alpha, \beta, v) = \int_0^x b(\phi, \alpha, \beta, v) d\phi = I_x(\alpha, \beta) = 1 - \bar{B}(x, \alpha, \beta, v), \quad (13)$$

where $I_x(\alpha, \beta)$ is the regularized incomplete beta function. Near the right endpoint, the properties of the upper-limit lognormal,

$$\lim_{x \rightarrow \infty} \frac{\bar{U}(v-r/x)}{\bar{U}(v-1/x)} = \begin{cases} \infty & r \in (1, +\infty) \\ 1 & \text{for } r = 1 \\ 0 & r \in (0, 1) \end{cases}, \quad (14)$$

are antisymmetric to those of the lognormal (8). On the other hand, near the right endpoint, the beta distribution is regularly varying,

$$\lim_{x \rightarrow \infty} \frac{\bar{B}(v-r/x)}{\bar{B}(v-1/x)} = r^{\beta-1}, \text{ where we assume } r > 0, \quad (15)$$

and so, as the right endpoint is approached, the beta distribution is similar to a power-law (7) (e.g., Embrechts et al., 1997, example 3.3.17). And, furthermore, in symmetry with Equation 9,

$$\lim_{x \rightarrow \infty} \frac{\bar{B}(v-1/x)}{\bar{U}(v-1/x)} = \infty. \quad (16)$$

In other words, for given fits to data, $\{\alpha, \beta, v\}$ and $\{\mu, \sigma, v\}$, extrapolated occurrence probabilities for intensities approaching the right endpoint will be higher for beta models than for upper-limit lognormal models.

9. Models for Block-Maximum Samples

As we discuss in Section 4, our ranked $-Dst_1$ and $-Dst_2$ data values are a solar cycle-by-cycle (block-by-block) down-sampling of the Dst time series. This removes most of the autocorrelation, giving us a dataset suitable for statistical analysis. But how are our hypotheses that magnetic storm intensities $-Dst_m$ might be the result of a lognormal or power-law source processes, or upper-limit lognormal or beta source processes, reflected in the statistical properties of the $-Dst_1$ and $-Dst_2$ samples? Extreme-value theory provides us with an answer to this question. Under the Fisher-Tippett-Gnedenko theorem (Albeverio & Piterbarg, 2006, Section 3.2.1; Davison & Huser, 2015, Section 2; Gomes & Guillou, 2015, Section 2.1), the generalized extreme-value distribution (GEV) (e.g., Bali, 2003; Walshaw, 2013) describes block maxima samples taken from an extremely wide variety of source distributions. For positive data $\{x\}$ that are GEV distributed, the probability density function is

$$\gamma(x, \mu, \sigma, \xi) = \begin{cases} \frac{1}{\sigma} \left(1 + \xi \frac{(x - \mu)}{\sigma} \right)^{\frac{1}{\xi} - 1} \exp \left[- \left(1 + \xi \frac{(x - \mu)}{\sigma} \right)^{\frac{1}{\xi}} \right] & \text{for } \xi \neq 0 \\ \frac{1}{\sigma} \exp \left(- \frac{x - \mu}{\sigma} \right) \exp \left[- \exp \left(- \frac{x - \mu}{\sigma} \right) \right] & \text{for } \xi = 0 \end{cases} \quad (17)$$

and the cumulative function is

$$\Gamma(x, \mu, \sigma, \xi) = \begin{cases} \exp \left[- \left(1 + \xi \frac{(x - \mu)}{\sigma} \right)^{\frac{1}{\xi}} \right] & \text{for } \left\{ \begin{array}{l} \xi \neq 0 \\ \xi = 0 \end{array} \right\} \\ \exp \left[- \exp \left(- \frac{x - \mu}{\sigma} \right) \right] & \end{cases} = 1 - \bar{\Gamma}(x, \mu, \sigma, \xi). \quad (18)$$

The GEV distribution has been applied in a diversity of scientific projects (e.g., Ghil et al., 2011), in statistical analyses of space-weather phenomena (e.g., O'Brien et al., 2007; Tsiftsi & De la Luz, 2018), and, in particular, in statistical analyses of magnetic storm intensities (e.g., Chen et al., 2019; Elvidge, 2020; Love, 2020; Nikitina et al., 2016; Woodroffe et al., 2016). The GEV distribution is certainly useful for parameter exploration. Since block-maximum samples taken from the tail of practically any source distribution can be modeled by the GEV distribution, it can also be used without hypothesizing a source process (Hewitt, 1970, p. 343), but this is something we want to avoid.

Formal statistical hypothesis testing can be performed by comparing special cases of the GEV distribution with data. Depending on the shape parameter, ξ , the GEV distribution reduces to one of three special cases,

$$\Gamma(x, \mu, \sigma, \xi) = \begin{cases} \text{Frechet: } F(x, \mu, \sigma, \xi) & x \in (\nu = \mu - \sigma / \xi, +\infty) & \xi > 0 \\ \text{Gumbel: } G(x, \mu, \sigma) & x \in (-\infty, +\infty) & \text{for } \xi = 0. \\ \text{Weibull: } W(x, \mu, \sigma, \xi) & x \in (-\infty, \nu = \mu - \sigma / \xi) & \xi < 0 \end{cases} \quad (19)$$

We note the scaling properties

$$\lim_{x \rightarrow \infty} \frac{\bar{F}(r \cdot x)}{\bar{F}(x)} = r^{-\frac{1}{\xi}} \text{ for } r > 0. \quad (20)$$

$$\lim_{x \rightarrow \infty} \frac{\bar{G}(r \cdot x)}{\bar{G}(x)} = \begin{cases} 0 & r \in (1, +\infty) \\ 1 & \text{for } r = 1 \\ \infty & r \in (0, 1) \end{cases}, \quad (21)$$

$$\lim_{x \rightarrow \infty} \frac{\bar{W}(v - r/x)}{\bar{W}(v - 1/x)} = r^{-\frac{1}{\xi}}, \text{ for } r > 0 \quad (22)$$

from which we understand that the Fréchet distribution is both domain-unlimited to the right and regularly varying at infinity. And, under the Fisher-Tippett-Gnedenko theorem, block-maximum samples taken from a right-unbounded source distribution that is regularly varying at infinity will be Fréchet distributed. The Weibull distribution is domain-right-limited, with maximum value at $v = \mu - \sigma/\xi$, and regularly varying at that right endpoint; samples taken from a right-limited source distribution that is regularly varying at its right endpoint will be Weibull distributed. The Gumbel distribution is right-unbounded and not regularly varying at infinity. Notably, samples taken from a right-unbounded distribution that is not regularly varying at infinity, or samples taken from a right-limited distribution that is not regularly varying at its right endpoint, will be Gumbel distributed (e.g., Albeverio & Piterbarg, 2006, Chapter 3.2.1; Alves & Neves, 2014).

In light of our discussion in Section 8, we understand that block-maximum samples from a power-law source distribution will be Fréchet distributed—the power-law distribution is said to be in the “domain of attraction” of the Fréchet distribution (e.g., Embrechts et al., 1997, Example 3.3.31; Ferreira, 2009; Walshaw, 2013). Block-maximum samples taken from a beta source distribution will be Weibull distributed—the beta distribution is in the Weibull domain of attraction. Block-maximum samples taken from either a lognormal distribution, or a upper-limit lognormal source distribution, will be Gumbel distributed—both the lognormal and upper-limit lognormal distributions are in the Gumbel domain of attraction. We note that the Fréchet and Gumbel distributions have both been used in some statistical analyses of magnetic storms (e.g., Silbergleit, 1997; Weigel & Baker, 2003). The Weibull distribution has also been used in some statistical analyses of magnetic storms (e.g., Gopalswamy, 2018; Morriña et al., 2019; Watari et al., 2001), though, so far as we can tell, without invoking a specific underlying source process.

10. Framework for Ranked Samples

For our statistical analysis, we need to develop a framework for ranked data. For pairs of samples $\{x_1 > x_2\}$, each taken from blocks of data, the conditional GEV probability density function for x_2 given x_1 is

$$\gamma_{2|1}(x_2|x_1) = \frac{\gamma(x_2)}{\Gamma(x_1)}, \quad (23)$$

and the joint density function for x_1 and x_2 is

$$\gamma_{1,2}(x_1, x_2) = \gamma_{2|1}(x_2|x_1) \cdot \gamma(x_1) = \frac{\gamma(x_1)\gamma(x_2)}{\Gamma(x_1)} \quad (24)$$

(e.g., Chandler, 1952; Nagaraja, 1982; Solow & Beet, 2004). The marginal density and cumulative functions for x_1 are just those of the GEV distribution,

$$\gamma_1(x_1) = \int_{-\infty}^{x_1} \gamma_{1,2}(x_1, \phi_2) d\phi_2 = \gamma(x_1) \quad (25)$$

and

$$\Gamma_1(x_1) = \Gamma(x_1). \quad (26)$$

For x_2 , the marginal density function is

$$\gamma_2(x_2) = \int_{x_2}^{+\infty} \gamma_{1,2}(\phi_1, x_2) d\phi_1 = \begin{cases} \gamma(x_2) \left(1 + \xi \frac{(x_2 - \mu)}{\sigma} \right)^{-\frac{1}{\xi}} \\ \gamma(x_2) \exp\left(-\frac{x_2 - \mu}{\sigma}\right) \end{cases}, \quad (27)$$

and the marginal cumulative function is

$$\Gamma_2(x_2) = \int_{-\infty}^{x_2} \gamma_2(\phi_2) d\phi_2 = \begin{cases} \Gamma(x_2) \left[1 + \left(1 + \xi \frac{(x_2 - \mu)}{\sigma} \right)^{-\frac{1}{\xi}} \right] \\ \Gamma(x_2) \left[1 + \exp\left(-\frac{x_2 - \mu}{\sigma}\right) \right] \end{cases}. \quad (28)$$

11. Maximum-Likelihood Estimation

We fit models to the solar-cycle-ranked $-Dst_1$ and $-Dst_2$ data listed in Table 1 using the maximum-likelihood method (e.g., Bohm and Zech, Chapter 6.5, 2010, Chapter 6.5; Roe, 2001, Chapter 13.2). We consider three different types of models: (1) a Gumbel model, obtained by fitting the parameters $\{\mu, \sigma\}$ with the shape parameter $\xi = 0$, (2) an unconstrained GEV model, obtained by fitting $\{\mu, \sigma, \xi\}$ with ξ treated as a free parameter, (3) a constrained Weibull model, obtained, as a special-case of a GEV model, by fitting $\{\mu, \sigma\}$ with ξ determined by $\mu - \sigma/\xi = \nu = 2500$ nT, the theoretical maximum intensity that could possibly be realized for a magnetic storm (Vasyliūnas, 2011). Each model fitted to the data maximizes the joint likelihood

$$\mathcal{L}(\mu, \sigma, \xi) = \prod_{i=1}^n A \cdot \gamma_{1,2}(-Dst_1^i, -Dst_2^i), \quad (29)$$

where the product is taken over n solar cycles. A is a normalizing factor,

$$A \int_{m_1}^{+\infty} \int_{m_2}^{+\infty} \gamma_{1,2}(\phi_1, \phi_2) d\phi_2 d\phi_1 = 1, \quad (30)$$

where $m_1 = \min\{-Dst_1^i\}$ and $m_2 = \min\{-Dst_2^i\}$, so that,

$$\frac{1}{A} = \begin{cases} 1 - \Gamma(m_1) - \left(1 + \xi \frac{(m_1 - \mu)}{\sigma} \right)^{-\frac{1}{\xi}} \Gamma(m_2) \\ 1 - \Gamma(m_1) - \exp\left(-\frac{m_1 - \mu}{\sigma}\right) \Gamma(m_2) \end{cases}. \quad (31)$$

We use a simplex algorithm (e.g., Press et al., 1992, Chapter 10.4) to maximize \mathcal{L} and, thereby, obtain the maximum-likelihood parameters.

12. Comparisons of Models

In Figure 2, we show complementary cumulatives of the $-Dst_1$ and $-Dst_2$ intensities for the 11 solar cycles 14–24 and complementary cumulatives of the Gumbel, \bar{G}_1 and \bar{G}_2 , the unconstrained GEV, $\bar{\Gamma}_1$ and $\bar{\Gamma}_2$, and the constrained Weibull, \bar{W}_1 and \bar{W}_2 models, each fitted using the joint probability density function, Equation 24. We also list in Figure 2 in tabular form Gumbel, GEV, and Weibull model estimates of the probabilities that solar-cycle maximum intensity $-Dst_1$ will exceed a range of thresholds, 500, 565, 600, ..., 1000 nT. The maximum-likelihood parameters for the Gumbel model are $\mu = 401$ nT, $\sigma = 128$ nT. From these parameters, we can calculate model moments (e.g., Forbes et al., 2011, Chapter 19): the mode of $-Dst_1$ (the most likely value) is μ ; the mean of $-Dst_1$ is $\mu + \epsilon\sigma = 475$ nT, where $\epsilon \simeq 0.577$ is the Euler-Mascheroni constant; the median of $-Dst_1$ is $\mu - \sigma \ln(\ln 2) = 448$ nT; for this model, the theoretical

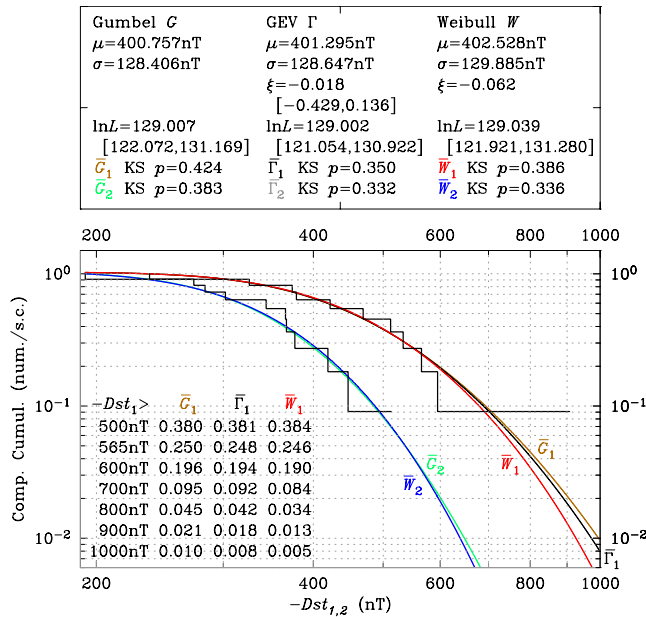


Figure 2. Complementary cumulatives of the cycle-ranked $-Dst_1$ and $-Dst_2$ data (solar cycles 14–24) and complementary cumulatives of fitted models: Gumbel G (green, brown), GEV Γ (black, gray, with ξ treated as a free parameter), and constrained Weibull W (red, blue, with ξ such that the right limit $\nu = 2500$ nT), each for parameters μ , σ , ξ that maximize the likelihood \mathcal{L} , Equation 29, for the joint density function given by 24. Also listed are the 68% confidence interval for ξ for the GEV model, log-likelihoods $\ln(\mathcal{L})$ for all three models, Kolmogorov-Smirnov p -values, separately for $-Dst_1$ and $-Dst_2$, and model estimates of the probabilities \bar{G}_1 , $\bar{\Gamma}_1$, and \bar{W}_1 that solar-cycle maximum intensity $-Dst_1$ will exceed a range of thresholds, 500 nT, ... 1000 nT.

means that that the cycle-ranked $-Dst_1$ and $-Dst_2$ data are, on a simple statistical basis, insufficient for discriminating between a ($\xi > 0$) right-unbounded, regularly varying Fréchet model, a ($\xi < 0$) right-limited, regularly varying Weibull model, or a ($\xi = 0$) right-unbounded, nonregularly varying Gumbel model.

The relative goodness of a model fitted to data is often measured by comparing likelihoods (e.g., Bohm & Zech, 2010, Chapter 10.3.4). The Gumbel, GEV, and Weibull models, respectively, have $\ln(\mathcal{L})$ of 129.007, 129.002, 129.039 (units, here, are not relevant). The Weibull model has the highest likelihood. To investigate whether or not this is significant, as before, we perform a bootstrap analysis, repeatedly sampling with replacement the solar-cycle $-Dst_1$ and $-Dst_2$ pairs, fitting models to each sample, and accumulating log-likelihood bootstrap sets $\{\ln(\mathcal{L})\}$ for each model type. From these sets, we obtain 68% confidence intervals on $\ln(\mathcal{L})$ for each model type. For the Weibull model, the interval is [121.921, 131.280], which is very wide compared to differences between the log-likelihoods of the three models. The intervals for the other models are similarly wide. From this, we understand that all three models are close to equally good representations of the cycle-ranked $-Dst_1$ and $-Dst_2$ data.

Next, we consider statistical significance. Would data that are statistically similar to those that we have be likely realizations of any of the fitted models? To answer this question, we turn, again, to the Kolmogorov-Smirnov test, but we recognize that it is circular to estimate significance with the same data used to estimate a model's parameters (e.g. Chave, 2017, Chapter 8.2.4; Corral & González, 2019, Section 3.2; Steinskog et al., 2007), therefore, we turn to bootstrap resampling. Treating each model as a “hypothesis,” we take multiple random bootstrap samplings with replacements of solar-cycle pairs $-Dst_1$ and $-Dst_2$, each time calculating a Kolmogorov-Smirnov p -value against the model. For each model, the median p -value of the resamplings is a suitable estimate of significance (e.g., Clauset et al., 2009, Section 3.4; Corral &

maximum value is infinite. The maximum-likelihood parameters of the unconstrained GEV model are $\mu = 401$ nT, $\sigma = 129$ nT, with a tiny shape parameter $\xi = -0.018$. From these parameters, we can calculate model moments: the mode of $-Dst_1$ is $\mu + (\sigma / \xi) \left[(1 + \xi)^{-\xi} - 1 \right] = 404$ nT; the mean of $-Dst_1$ is $\mu + (\sigma / \xi) \left[\Gamma(1 - \xi) - 1 \right] = 473$ nT, where Γ is the Gamma function; the median of $-Dst_1$ is $\mu + (\sigma / \xi) \left[(\ln(2))^{-\xi} - 1 \right] = 448$ nT; each of these GEV moments is very similar to the corresponding Gumbel moments. Perhaps more interesting is the fact that the GEV estimated ξ is slightly negative. This implies a Weibull-type distribution with a maximum storm intensity of $\mu - \sigma/\xi = 7522$ nT, far higher than the theoretical maximum of 2500 nT. The maximum-likelihood parameters of the constrained Weibull model, with a maximum storm intensity set at 2500 nT, are $\mu = 403$ nT, $\sigma = 130$ nT, $\xi = -0.062$, for which the mode is 411 nT, the mean is 470 nT, and the median is 450 nT.

Qualitatively, all three models are good representations of the data, especially when considering the data's scatter. Among the three models, the Gumbel shows the heaviest distributional tail. The constrained Weibull model shows the lightest distributional tail. The tail of the unconstrained GEV model is tucked in between the tails of the Weibull and Gumbel models. Given these simple observations, one might reasonably wonder whether or not standard statistical tests can actually tell us which of the three models is best. Bootstrap resampling (e.g. Boos, 2003; Efron & Tibshirani, 1993) can quantify model uncertainty. We take solar-cycle $-Dst_1$ and $-Dst_2$ pairs as a population, which we sample with replacement. We fit each sample with a GEV model, obtaining, in each case, a new estimate of the shape parameter ξ . From numerous resamplings and refittings, we obtain a bootstrap set $\{\xi\}$. The (centered) 68% confidence interval is $[-0.429, 0.136]$. This statistical spread is wide enough that we cannot be especially confident in the $\xi = -0.018$ estimate for the shape parameter. That the 68% interval ranges from negative to positive values

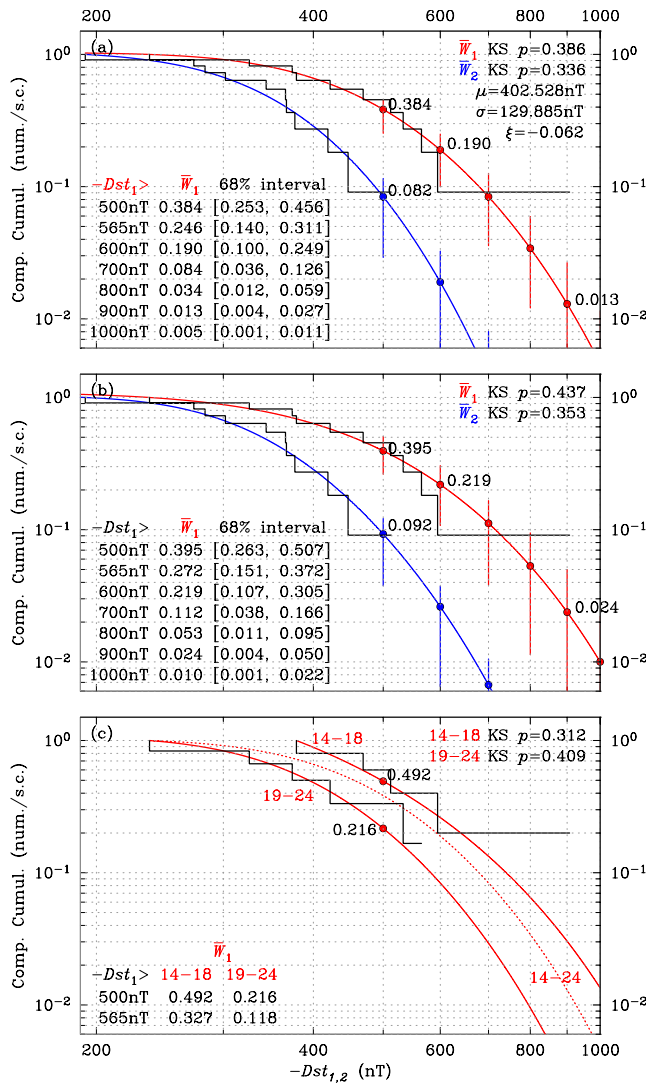


Figure 3. Complementary cumulatives of the cycle-ranked $-Dst_1$ and $-Dst_2$ data and complementary cumulatives of fitted constrained Weibull W (red, blue), each for parameters μ , σ , ξ that maximize the likelihood \mathcal{L} , Equation 29, with ξ such that the right limit $v = 2500$ nT. (a) Models fitted to $-Dst_1$ and $-Dst_2$ (solar cycles 14–24) and using the joint density function given by 24. (b) Models are fitted independently to $-Dst_1$ and $-Dst_2$ (cycles 14–24) using the non-joint density function given by 17. (c) Models fitted to $-Dst_1$ and $-Dst_2$ (separately for cycles 14–18, cycles 19–24, and cycles 14–24 as dashed line) using the joint density function given by 24; here, for purposes of clarity, fits to $-Dst_2$ are not shown. Listed are model estimates of the probabilities \bar{W}_1 that solar-cycle maximum intensity $-Dst_1$ will exceed a range of thresholds, 500 nT, ... 1000 nT, corresponding 68% confidence intervals, and Kolmogorov-Smirnov p -values, separately for $-Dst_1$ and $-Dst_2$.

González, 2019, Section 3.2; Steinskog et al., 2007). The median p -values for $-Dst_1$ and for the Gumbel, GEV, and Weibull models are, respectively, 0.424, 0.350, 0.386; for $-Dst_2$, they are 0.383, 0.332, 0.336. These probabilities are not small enough to motivate rejection of any of the three models as descriptions of the cycle-ranked $-Dst_1$ and $-Dst_2$ data.

Since the statistical tests do not allow us to confidently discriminate between the various extreme-value models, we understand that we cannot draw inferences about the nature of the source distribution. As far as we can tell, any one of power-law, lognormal, upper-limit lognormal, or beta sources could give the $-Dst_m$ from which we block sample for $-Dst_1$ and $-Dst_2$ data values. At this point, we recall the challenges we discuss in Section 6 in identifying the most intense storms for solar cycles 14–16. There, we accepted the fact that our compiled $-Dst_1$ and $-Dst_2$ data values for cycles 14–16 should be regarded as lower bounds because there is a (possibly slim) chance that we missed more intense storms. Bearing that in mind, we note, from Figure 2, that this choice makes little difference for storm intensities across a range of, say, 500–700 nT—all three models give similar $-Dst_1$ probabilities across that range. On the other hand, for greater storm intensities, such as $-Dst_1 > 900$ nT, differences between the three models are more significant. For a storm as intense as $-Dst_1 > 1000$ nT, the Gumbel model gives an occurrence probability of 0.010/cycle. The constrained Weibull model gives an occurrence probability of 0.005/cycle, half that of the Gumbel. Therefore, seeking not to exaggerate the storm probabilities, in what follows, we chose to emphasize results from the model that gives the lowest extreme-value storm probabilities: the Weibull model that is constrained to be right-limited for storm intensities at 2500 nT.

13. Storm Occurrence Rates

In Figure 3a, we show complementary cumulatives of the $-Dst_1$ and $-Dst_2$ intensities for solar cycles 14–24 and complementary cumulatives of the constrained Weibull model, \bar{W}_1 and \bar{W}_2 , fitted using the joint probability density function, Equation 24. We list in tabular form Weibull-model estimates of the probabilities \bar{W}_1 that solar-cycle maximum intensity $-Dst_1$ will exceed a range of thresholds, 500, 565, 600, ..., 1000 nT. We also show and list the corresponding 68% confidence intervals obtained from bootstrap resampling of $-Dst_1$ and $-Dst_2$ pairs and fitting a Weibull model to each sampling. Note, in particular, the probability that $-Dst_1$ will exceed 500 nT is $\bar{W}_1 = 0.384$ /cycle, corresponding to an average return rate of just 2.6 solar cycles. The corresponding 68% confidence interval is [0.253, 0.456]/cycle. In Figure 3b, we show Weibull models fitted, independently, to the $-Dst_1$ intensities and the $-Dst_2$ intensities, using a likelihood function constructed from the (nonjoint) Weibull density function given by Equation 17. As noted by Solow and Beet (2004), a nonjoint fitting does not exploit the information content of ordering in the data, that is, the information content of the conditional probability of $-Dst_2$ given $-Dst_1$; but this is essentially what was done in some previous investigations (e.g., Siscoe, 1976a; Willis et al., 1997). For $-Dst_1 > 500$ nT storms, the probability of the nonjoint model is $\bar{W}_1 = 0.395$ /cycle, which is similar to the 0.384/cycle value obtained for the joint model, Figure 3a. Differences are greater farther out on the Weibull tail. For $-Dst_1 > 1000$ nT storms, the nonjoint probability is $\bar{W}_1 = 0.010$ /cycle, or twice as high as the 0.005/cycle value obtained for the joint model. Evidently, the

investigations (e.g., Siscoe, 1976a; Willis et al., 1997). For $-Dst_1 > 500$ nT storms, the probability of the nonjoint model is $\bar{W}_1 = 0.395$ /cycle, which is similar to the 0.384/cycle value obtained for the joint model, Figure 3a. Differences are greater farther out on the Weibull tail. For $-Dst_1 > 1000$ nT storms, the nonjoint probability is $\bar{W}_1 = 0.010$ /cycle, or twice as high as the 0.005/cycle value obtained for the joint model. Evidently, the

joint-probability model, Figure 3a, gives more conservative estimates of future superstorm occurrence probabilities than the nonjoint model, Figure 3b.

In Figure 3c, we show results for a bisection test, fitting $-Dst_1$ and $-Dst_2$ separately for solar cycles 14–18 and for cycles 19–24; for clarity, we only show complementary cumulatives for $-Dst_1$ and \bar{W}_1 even though, as in Figure 3a, we are fitting Weibull models using the joint density function that includes $-Dst_2$. We recall, from Section 7, that neither a Kolmogorov-Smirnov test nor a Student's t test is sufficient to reject the possibility that $-Dst_1$ and $-Dst_2$ values from cycles 14–18 and values from cycles 19–24 are both taken the same distribution. Still, in Figure 3c, we see practical differences in the fitted Weibull models. For cycles 14–18, the probability of a $-Dst_1 > 500$ nT storm is 0.492/cycle, but for cycles 19–24 the probability is 0.216/cycle. As we have already noted, from Figure 3a, modeling data for cycles 14–24 (inclusive of several intense pre-IGY storms) yields a probability for $-Dst_1 > 500$ nT storm of 0.384/cycle. This is 78% higher than the probability (0.216/cycle) obtained by only modeling data for cycles 19–24. We recall from Section 6 that $-Dst_1$ and $-Dst_2$ for cycles 14–16 should be regarded as lower bounds. If there were storms more intense for those cycles, more intense than we list in Table 1, then the methods we use here would yield higher $-Dst_1 > 500$ nT probabilities.

14. Probability of 1859, 1921, 1989 Storms

The Carrington event of September 1859 is recognized as a superstorm (e.g., Cliver & Dietrich, 2013; Hayakawa, Ebihara, Wills, et al., 2019). It brought widespread interference to telegraph systems (e.g., Boteler, 2006) and caused low-latitude aurora (e.g., Green et al., 2006), but its absolute intensity is uncertain. Only one low-latitude observatory, that of Colaba (CLA), India, reported a complete record of the storm (Tsurutani et al., 2003). The CLA record has been used to estimate a peak Carrington intensity of $-Dst_1 = 850$ nT (Siscoe et al., 2006) and $-Dst_1 = 1050$ nT (Gonzalez et al., 2011), even though it is understood that local-time asymmetry in low-latitude geomagnetic disturbance, caused, for example, by field-aligned currents, can result in local disturbance being low or high relative to a mean disturbance level from multiple observatories. If we accept the intensity estimates for the Carrington event, then it and the magnetic storm of May 1921 are the only two storms over the past 15 solar cycles (10 through 24) with $-Dst_1 > 900$ nT. From our Weibull model, a storm of such intensity has an occurrence probability of $\bar{W}_1 = 0.013$ /cycle (average return rate of 76.9 cycles). That is a low probability, something also noted by Moriña et al. (2019).

For perspective, we note that the bootstrap (centered) 68% confidence interval on the Weibull occurrence probability for storms with $-Dst_1 > 900$ nT, from Figure 3a, is [0.004, 0.027]/cycle. The upper threshold on this interval, 0.027/cycles, corresponds to a return rate of 37.0 cycles. The 68% confidence interval means that there is a one-sided probability of 16% that the per-cycle probability is greater than 0.027/cycles (and that the return rate is less than 37.0 cycles). A more rigorous check can be obtained with a Kolmogorov-Smirnov test. Here, we use the Weibull model fitted to the $-Dst_1$ and $-Dst_2$ data from cycles 14–24, exactly as in Figure 3a, but, for the Kolmogorov-Smirnov test, we add a 12th $-Dst_1$ value of 850 nT, similar to the Carrington intensity. Then, as in Section 12, we obtain a set of bootstrap p -values. The median of these is 0.325, only slightly lower than the 0.386 median value obtained using only data from cycles 14–24. This is not small enough to motivate the Weibull model's rejection, even for a rare Carrington intensity. In this light, and recalling that we chose to focus on Weibull models because they give lower maximum-likelihood probabilities than the Gumbel and unconstrained GEV models, we understand that the historical occurrence of the Carrington event cannot be viewed as necessarily inconsistent with our modeling.

Regarding the March 1989 storm ($-Dst_1 = 565$ nT), the most intense storm since the IGY, we note from Table 1 that, over solar cycles 14–24, only the September 1909 and May 1921 storms had, to our knowledge, higher intensities. In extending the span of $-Dst_1$ and $-Dst_2$ from solar cycles 19–24 (IGY and afterward) to cycles 14–24 (inclusive of several pre-IGY superstorms), from Figures 3a and 3c, our estimate of the probability of a $-Dst_1 > 565$ nT storm is higher by 126%, from 0.118/cycle (average return rate of 8.47 cycles) to 0.246/cycle (return rate of 4.1 cycles). We recall from Section 6, that our $-Dst_1$ and $-Dst_2$ intensities for cycles 14–16 should be regarded as lower bounds. If there were storms more intense for those cycles, then the methods we use here would yield a higher probability for the occurrence of a 1989-like storm. For now, we can say that previous suggestions that the March 1989 storm was, essentially, a once-per-century storm

(e.g., Boteler, 2019; Love et al., 2018; Pulkkinen et al., 2012) appear to be “optimistic”—a storm of such intensity apparently occurs about every 45 years.

15. Once-Per-Century Storm Intensity

To estimate storm intensity for a given exceedance probability, we invert Equation 18 to obtain the quantile function,

$$x(\bar{\Gamma}, \mu, \sigma, \xi) = \begin{cases} \mu + \frac{\sigma}{\xi} \left[\left(-\ln(1 - \bar{\Gamma}) \right)^{-\xi} - 1 \right] & \text{for } \left(\begin{array}{l} \xi \neq 0 \\ \xi = 0 \end{array} \right) \\ \mu - \sigma \ln \left[-\ln(1 - \bar{\Gamma}) \right] \end{cases} \quad (32)$$

We can use this to estimate the intensity of a “once-per-century” storm. Assuming that each solar cycle is 11 years in duration, 9 cycles equals about 99 years. For $\bar{\Gamma} = 1/9$ and using the maximum-likelihood parameters for the Weibull model obtained by fitting $-Dst_1$ and $-Dst_2$ for solar cycles 14–24, we obtain a once-per-century intensity of $-Dst_1 = 663$ nT and a corresponding bootstrap 68% confidence interval of [497, 694] nT. We recall, again, the ambiguity in the rankings of storm intensities for cycles 14–16. Using our methods with storms more intense for cycles 14–16 would yield a higher once-per-century storm intensity.

16. Discussion and Conclusions

Our cycle-ranked extreme-event analysis of $-Dst_1$ and $-Dst_2$ represents a more complete exploitation of the available data than previous analyses that only use cycle-maxima $-Dst_1$ (e.g., Love, 2020; Silbergleit, 1997). Our extension of the number of solar-cycle ranked $-Dst_m$ intensities to cover cycles 14–24 (1902–2016) is, we might expect, a better representation of extreme-value storm intensities than the $-Dst_m$ values taken from shorter intervals, such as the post-IGY interval covering cycles 19–24 (1957–2016) and used in some previous analyses (e.g., Love, 2020; Riley & Love, 2017; Silbergleit, 1997; Tsubouchi & Omura, 2007; Yermolaev et al., 2013). Notably, the extended dataset encompasses several storms with $-Dst_m > 500$ nT (1903, 1909, 1921, 1946) that occurred before 1957, whereas only two such storms (1989 and 2003) occurred after 1957. Although significance tests tell us that we cannot reject the possibility that this difference is just a statistical fluke, Section 7, the difference is real, and it affects estimates of the occurrence probabilities of future intense storms. We recall, for example, from Section 14 and Figure 3, that using the extended dataset yields a maximum-likelihood probability for a storm as intense as that of 1989 of 0.246/cycle (return rate of 4.1 cycles). This is more than twice as high as the probability obtained using the same methods and the shorter standard 1957–2016 dataset.

Such results generate interest in obtaining additional estimates of storm intensities. We recall, from Section 6, that there is some (possibly slight) ambiguity in the rankings of storm intensities for cycles 14–16. This ambiguity is why we have noted that, using the same methods, but storms more intense than those identified for cycles 14–16, would yield a higher once-per-century intensity and a higher probability for a $-Dst_m > 565$ nT storm. Opportunities for improvement in statistical analyses like that reported here might come by pushing the storm-intensity compilation back to even earlier solar cycles, though this entails challenges. Consider, for example, solar cycle 13. The storm of February 1892, $AA_1^* = 249.6$ nT, was one of that cycle’s most intense storms (e.g., Superintendent of the U.S. Naval Observatory, 1892). It was completely recorded at Colaba (CLA), India (Moos, 1910, Plate 81 D), San Fernando (SFS), Spain (Instituto y Observatorio de Marina, 1893), and Zi-Ka-Wei (ZKW), China. In contrast, the storm of August 1894 (e.g., Finn, 1894), $AA_3^* = 193.6$ nT, was completely recorded at CLA (Moos, 1910, Plate 81 H), but it was not at SFS and not at ZKW, per yearbooks. We know of no observatory record for either of these storms from the American sector. One could probably reliably estimate $-Dst_m$ for the first storm, but, with a recording from only one observatory, estimating $-Dst_m$ for the second storm is more problematic.

Finally, from Section 8, we recall our discussion of several candidate stochastic source processes that might describe storm-maximum intensities. On physical grounds, we prefer those source processes with associat-

ed distributions that are right-limited—storms of infinite intensity are not possible, and so the distribution describing extreme storm intensities should reasonably accommodate an upper limit. Such distributions might be either regularly varying, a property that can arise from self-organized critical processes, or they might be nonregularly varying, a property that can arise from the multiplicative action of multiple random processes. We recall, from Section 9, that block samples of right-limited, regularly varying data are Weibull distributed, while block samples from right-limited, non-regularly varying data are Gumbel distributed (though the Gumbel, itself, is not right-limited). And we recall, from Section 12 and Figure 2, that a Gumbel model and a Weibull model (one constrained to have a theoretical upper limit of 2500 nT) both provide good representations of the cycle-ranked $-Dst_1$ and $-Dst_2$ data, and, therefore, we are not able to discriminate between source processes that are regularly varying or not regularly varying. This issue is important for accurately predicting the probabilities of the most extremely intense magnetic storms, differences in the far-end tails of the candidate models, for storm intensities of (say) $-Dst_1 > 1000$ nT, can be a factor of two. Seeking not to overstate storm probabilities, we chose to emphasize the constrained Weibull model in this report since it gives lower probabilities than the Gumbel. We wonder if physics-based theories or simulations might better inform the most appropriate statistical model of extreme-value storm intensities or the theoretical upper-limit on storm intensity. If we knew that the Gumbel model is appropriate for cycle ranked $-Dst_m$, possibly because the source distribution is upper-limit lognormal, then the probabilities of the most extreme storms, estimated using the data in Table 1, would be higher than those reported here. On the other hand, if we knew that the Weibull model is appropriate, but that the theoretical upper limit on storm intensity is less than the 2500 nT that Vasyliūnas (2011) estimates, then the probabilities of the most extreme storms, estimated using the data in Table 1, would be lower than those reported here. Either way, we see opportunities for physics-based theories to further advance statistical analyses of extremely intense magnetic storms and to better predict the probabilities of their future occurrences.

Data Availability Statement

The standard *Dst* index is available from the Kyoto WDC (wdc.kugi.kyoto-u.ac.jp). The Oulu *Dst* index is available from the University of Oulu, Finland (dcx oulu.fi). Historical observatory hourly data are available from the Kyoto WDC and the Edinburgh WDC (www.wdc.bgs.ac.uk). We used observatory yearbooks from the USGS, the National Oceanic and Atmospheric Administration, the Linda Hall Library, Kansas City, Missouri, the National Diet Library Digital Collections, Japan (dl.ndl.go.jp), and google.com. The homogeneous *aa* index is available as a supplement to Lockwood, Chambodut, et al. (2018) (<https://doi.org/10.1051/swsc/2018038>). Sunspot numbers are available from the WDC-SILSO (sidc.be/silso), Royal Observatory of Belgium, Brussels.

Acknowledgments

The authors thank E. W. Cliver, K. A. Lewis, E. J. Rigler, B. R. Shiro, J. L. Slate, and three anonymous individuals (journal reviewers) for reviewing a draft manuscript. This work was supported by the U.S. Geological Survey Geomagnetism Program. We thank the USGS Library for support in obtaining documents.

References

- Albeverio, S., & Piterbarg, V. (2006). Mathematical methods and concepts for the analysis of extreme events. In S. Albeverio, V. Jentsch, & H. Kantz (Eds.), *Extreme events in nature and society* (pp. 47–68), Springer: Berlin, Germany.
- Allen, J., Sauer, H., Frank, L., & Reiff, P. (1989). Effects of the March 1989 solar activity. *Eos, Transactions American Geophysical Union*, 70(46), 1479–1488, 1479. <https://doi.org/10.1029/89EO00409>
- Alves, I. F., & Neves, C. (2014). Estimation of the finite right endpoint in the Gumbel domain. *Statistica Sinica*, 24, 1811–1835. <https://doi.org/10.5705/ss.2013.183>
- Angelopoulos, V., Mukai, T., & Kokubun, S. (1999). Evidence for intermittency in Earth's plasma sheet and implications for self-organized criticality. *Physics of Plasmas*, 6, 4161–4168. <https://doi.org/10.1063/1.873681>
- Angenheister, G., & Westland, C. J. (1921). The magnetic storm of May 13-16, 1921, at Apia Observatory, Samoa. *Journal of Geophysical Research*, 26(1-2), 30–31. <https://doi.org/10.1029/TE026i001p0030>
- Aschwanden, M. (2011). *Self-organized criticality in astrophysics: The statistics of nonlinear processes in the universe*. Chichester, UK: Praxis Publishing.
- Astafyeva, E., Yasyukevich, Y., Maksikov, A., & Zhivetiev, I. (2014). Geomagnetic storms, super-storms, and their impacts on GPS-based navigation systems. *Space Weather*, 12(7), 508–525. <https://doi.org/10.1002/2014SW001072>
- Baker, D. N. (2002). How to cope with space weather. *Science*, 297(5586), 1486–1487. <https://doi.org/10.1126/science.1074956>
- Baker, D. N., Balstad, R., Bodeau, J. M., Cameron, E., Fennell, J. E., Fisher, G. M., et al. (2008). Severe Space Weather Events – Understanding Societal and Economic Impacts, 1–144. Washington, DC: The National Academy Press. <https://doi.org/10.17226/12507>
- Balasis, G., Daglis, I. A., Papadimitriou, C., Kalimeri, M., Anastasiadis, A., & Eftaxias, K. (2009). Investigating dynamical complexity in the magnetosphere using various entropy measures. *Journal of Geophysical Research*, 114, A00D06. <https://doi.org/10.1029/2008JA014035>
- Balch, C., Murtagh, B., Zezula, D., Combs, L., Nelson, G., Tegnell, K., et al. (2004). *Service assessment: Intense space weather storms October 19 - November 07, 2003* (pp. 1–49). Silver Spring, MD: US Dept. Commerce, NOAA.

- Bali, T. G. (2003). The generalized extreme value distribution. *Economics Letters*, 79(3), 423–427. [https://doi.org/10.1016/S0165-1765\(03\)00035-1](https://doi.org/10.1016/S0165-1765(03)00035-1)
- Barnes, P. R., Rizy, D. T., McConnell, B. W., Tesche, F. M., & Taylor, E. R., Jr (1991). In *Oak Ridge Nat. Lab. Electric Utility Industry Experience with Geomagnetic Disturbances*, ORNL-6665 (pp. 1–78). Oak Ridge, TN: Oak Ridge National Laboratory.
- Basu, S., Basu, S., MacKenzie, E., Bridgwood, C., Valladares, C. E., Groves, K. M., & Carrano, C. (2010). Specification of the occurrence of equatorial ionospheric scintillations during the main phase of large magnetic storms within solar cycle 23. *Radio Science*, 45(5). <https://doi.org/10.1029/2009RS004343>
- Bell, J. T., Gussenhoven, M. S., & Mullen, E. G. (1997). Super storms. *Journal of Geophysical Research*, 102(A7), 14189–14198. <https://doi.org/10.1029/96JA03759>
- Bezdek, J. C., & Solomon, K. H. (1983). Upper limit lognormal distribution for drop size data. *Journal of Irrigation and Drainage Engineering*, 109(1), 72–88. [https://doi.org/10.1061/\(ASCE\)0733-9437\(1983\)109:1\(72\)](https://doi.org/10.1061/(ASCE)0733-9437(1983)109:1(72))
- Bohm, G., & Zech, G. (2010). *Introduction to statistics and data analysis for physicists* (pp. 1–398). Hamburg, Germany: Verlag Deutsches Elektronen-Synchrotron.
- Bolduc, L. (2002). GIC observations and studies in the Hydro-Québec power system. *Journal of Atmospheric and Solar-Terrestrial Physics*, 64(16), 1793–1802. [https://doi.org/10.1016/S1364-6826\(02\)00128-1](https://doi.org/10.1016/S1364-6826(02)00128-1)
- Boos, D. D. (2003). Introduction to the bootstrap world. *Statistical Science*, 18(2), 168–174. <https://doi.org/10.1214/ss/1063994971>
- Borovsky, J. E. (2020). What magnetospheric and ionospheric researchers should know about the solar wind. *Journal of Atmospheric and Solar-Terrestrial Physics*, 204(11), 105271–271. <https://doi.org/10.1016/j.jastp.2020.105271>
- Borovsky, J. E., & Shprits, Y. Y. (2017). Is the Dst index sufficient to define all geospace storms? *Journal of Geophysical Research - A: Space Physics*, 122(11), 11543–11547. <https://doi.org/10.1002/2017JA024679>
- Boteler, D. H. (2006). The super storms of August/September 1859 and their effects on the telegraph system. *Advances in Space Research*, 38(2), 159–172. <https://doi.org/10.1016/j.asr.2006.01.013>
- Boteler, D. H. (2019). A 21st century view of the March 1989 magnetic storm. *Space Weather*, 17(10), 1427–1441. <https://doi.org/10.1029/2019SW002278>
- Bowman, B. R., Tobiska, W. K., Marcos, F. A., Huang, C. Y., Lin, C. S., & Burke, W. J. (2008). A new empirical thermospheric density model JB2008 using new solar and geomagnetic indices. In *AIAA/AAS Astrodynamics Specialist Conference and Exhibit* (pp. 1–19), 2008-6438. <https://doi.org/10.2514/6.2008-6438>
- Burlaga, L. F. (2001). Lognormal and multifractal distributions of the heliospheric magnetic field. *Journal of Geophysical Research*, 106(A8), 15917–15927. <https://doi.org/10.1029/2000JA000107>
- Burlaga, L. F., & Lazarus, A. J. (2000). Lognormal distributions and spectra of solar wind plasma fluctuations: Wind 1995–1998. *Journal of Geophysical Research*, 105(A2), 2357–2364. <https://doi.org/10.1029/1999JA900442>
- Cannon, P., Angling, M., Barclay, L., Curry, C., Dyer, C., Edwards, R., et al. (2013). *Extreme space weather: Impacts on engineered systems and infrastructure* (pp. 1–68). Royal Academy of Engineering, London, UK.
- Chandler, K. N. (1952). The distribution and frequency of record values. *Journal of the Royal Statistical Society: Series B*, 14(2), 220–228. <https://doi.org/10.1111/j.2517-6161.1952.tb00115.x>
- Chang, T. (1999). Self-organized criticality, multi-fractal spectra, sporadic localized reconnections and intermittent turbulence in the magnetotail. *Physics of Plasmas*, 6, 4137–4145. <https://doi.org/10.1063/1.873678>
- Chapman, S. C., McIntosh, S. W., Leamon, R. J., & Watkins, N. W. (2020). Quantifying the solar cycle modulation of extreme space weather. *Geophysical Research Letters*, 47(11) e2020GL087795. <https://doi.org/10.1029/2020GL087795>
- Chave, A. D. (2017). *Computational statistics in the Earth sciences* (pp. 1–451). Cambridge University Press, Cambridge, UK.
- Chen, S., Chai, L., Xu, K., Wei, Y., Rong, Z., & Wan, W. (2019). Estimation of the occurrence probability of extreme geomagnetic storms by applying extreme value theory to Aa index. *Journal of Geophysical Research: Space Physics*, 124(12), 9943–9952. <https://doi.org/10.1029/2019JA026947>
- Clauset, A., Shalizi, C. R., & Newman, M. E. J. (2009). Power-law distributions in empirical data. *SIAM Review*, 51(4), 661–703. <https://doi.org/10.1137/070710111>
- Clette, F., Svalgaard, L., Vaquero, J. M., & Cliver, E. W. (2014). Revisiting the sunspot number. *Space Science Reviews*, 186, 35–103. <https://doi.org/10.1007/s11214-014-0074-2>
- Cliver, E. W., Balasubramaniam, K. S., Nitta, N. V., & Li, X. (2009). Great geomagnetic storm of 9 November 1991: Association with a disappearing solar filament. *Journal of Geophysical Research - A: Space Physics*, 114(A3) A00A20. <https://doi.org/10.1029/2008JA013232>
- Cliver, E. W., & Dietrich, W. F. (2013). The 1859 space weather event revisited: Limits of extreme activity. *Journal of Space and Weather Space Climate*, 3, A31. <https://doi.org/10.1051/swsc/2013053>
- Coles, S. (2001). *An introduction to statistical modeling of extreme values* (pp. 1–224). London, UK: Springer-Verlag.
- Corral, Á., & González, A. (2019). Power law size distributions in geoscience revisited. *Earth and Space Science*, 6(5), 673–697. <https://doi.org/10.1029/2018EA000479>
- Daglis, I. A. (2006). Ring current dynamics. *Space Science Reviews*, 124(1–4), 183–202. <https://doi.org/10.1007/s11214-006-9104-z>
- Daglis, I. A., Kozyra, J. U., Kamide, Y., Vassiliadis, D., Sharma, A. S., Liemohn, M. W., et al. (2003). Intense space storms: Critical issues and open disputes. *Journal of Geophysical Research: Space Physics*, 108(A5), 1208. <https://doi.org/10.1029/2002JA009722>
- Davison, A. C., & Huser, R. (2015). Statistics of extremes. *Annual Review of Statistics and its Application*, 2, 203–235. <https://doi.org/10.1146/annurev-statistics-010814-020133>
- Eastwood, J. P., Biffis, E., Hapgood, M. A., Green, L., Bisi, M. M., Bentley, R. D., et al. (2017). The economic impact of space weather: Where do we stand?. *Risk Analysis*, 37(2), 206–218. <https://doi.org/10.1111/risa.12765>
- Ebihara, Y., & Ejiri, M. (1998). Modeling of solar wind control of the ring current buildup: A case study of the magnetic storms in April 1997. *Geophysical Research Letters*, 25(20), 3751–3754. <https://doi.org/10.1029/1998GL900006>
- Echer, E., Gonzalez, W. D., & Tsurutani, B. T. (2011). Statistical studies of geomagnetic storms with peak Dst ≤ -50 nT from 1957 to 2008. *Journal of Atmospheric and Solar-Terrestrial Physics*, 73(11–12), 1454–1459. <https://doi.org/10.1016/j.jastp.2011.04.021>
- I. A. Daglis (Ed.), (2005). *Effects of space weather on technology infrastructure* (pp. 1–334). The Netherlands: Springer.
- E. L. Crow, & K. Shimizu (Eds.), (1988). *Lognormal distributions: Theory and applications* (pp. 1–387). New York, NY: Marcel Dekker.
- Efron, B., & Tibshirani, R. J. (1993). *An introduction to the bootstrap*. Dordrecht, The Netherlands: Springer Science+Business Media.
- Elvidge, S. (2020). Estimating the occurrence of geomagnetic activity using the Hilbert-Huang transform and extreme value theory. *Space Weather*. e2020SW002. <https://doi.org/10.1029/2020SW002513>
- Embrechts, P., Klüppelberg, C., & Mikosch, T. (1997). *Modeling extremal events: For Insurance and finance, applications of mathematics: stochastic modeling and applied probability* (pp. 1–648). Springer-Verlag, Berlin, Germany.

- Faris, R. L. (1920). Magnetic storm of August 11-12, 1919, as recorded at the Honolulu Magnetic Observatory. *Journal of Geophysical Research*, 25(1), 14. <https://doi.org/10.1029/TE025i001p00014-01>
- Ferreira, A. (2009). Extreme values in reliability. In E. L. Melnick, & B. S. Everitt (Eds.), *Encyclopedia of quantitative risk analysis and assessment* (pp. 686–691). Chichester, UK: John Wiley & Sons.
- Finn, W. (1894). Recent observations on Earth currents. *Electrical Engineer*, 18(3), 161.
- Fleming, J. A., Johnston, H. F., Forbush, S. E., McNish, A. G., Scott, E., & W (1947). Magnetic Results from Watheroo Observatory, Western Australia, 1919-1935 (VII-A (pp. 1–1122). Carnegie Institution of Washington: Washington, DC, 1919-1935.
- Forbes, C., Evans, M., Hastings, N., & Peacock, B. (2011). *Statistical distributions*. Hoboken, NJ: John Wiley & Sons.
- Ganushkina, N., Jaynes, A., & Liemohn, M. (2017). Space weather effects produced by the ring current particles. *Space Science Reviews*, 212, 1315–1344. <https://doi.org/10.1007/s11214-017-0412-2>
- Ghil, M., Yiou, P., Hallegatte, S., Malamud, B. D., Naveau, P., Soloviev, A., et al. (2011). Extreme events: Dynamics, statistics and prediction. *Nonlinear Processes in Geophysics*, 18(3), 295–350. <https://doi.org/10.5194/npg-18-295-2011>
- Gomes, M. I., & Guillou, A. (2015). Extreme value theory and statistics of univariate extremes: A review. *International Statistical Review*, 83(2), 263–292. <https://doi.org/10.1111/insr.12058>
- Gonzalez, W. D., Echer, E., Tsurutani, B. T., Clúa de Gonzalez, A. L., & Dal Lago, A. (2011). Interplanetary origin of intense, superintense and extreme geomagnetic storms. *Space Science Reviews*, 158(1), 69–89. <https://doi.org/10.1007/s11214-010-9715-2>
- Gonzalez, W. D., Joselyn, J. A., Kamide, Y., Kroehl, H. W., Rostoker, G., Tsurutani, B. T., & Vasyliunas, V. M. (1994). What is a geomagnetic storm?. *Journal of Geophysical Research*, 99(A4), 5771–5792. <https://doi.org/10.1029/93JA02867>
- Gopalswamy, N. (2018). Extreme solar eruptions and their space weather consequences. In N. Buzulukova (Ed.), *Extreme space weather: Origins, predictability, and consequences* (pp. 37–63). Amsterdam, The Netherlands: Elsevier, chap. 2.
- Gopalswamy, N., Akiyama, S., Yashiro, S., & Mäkelä, P. (2010). Coronal mass ejections from sunspot and non-sunspot regions. In S. Hasan, & R. Rutten (Eds.), *Magnetic coupling between the interior and atmosphere of the sun* (pp. 289–307), Berlin, Germany: Springer.
- Gopalswamy, N., Barbieri, L., Cliver, E. W., Lu, G., Plunkett, S. P., & Skoug, R. M. (2005). Introduction to violent Sun-Earth connection events of October-November 2003. *Journal of Geophysical Research*, 110. <https://doi.org/10.1029/2005JA011268>
- Green, J. L., Boardsen, S., Odenwald, S., Humble, J., & Pazamickas, K. A. (2006). Eyewitness reports of the great auroral storm of 1859. *Advances in Space Research*, 38(2), 145–154. <https://doi.org/10.1016/j.asr.2005.12.021>
- Green, L. M., Deighton, R., & Baker, D. (2016). *Building space weather resilience in the finance sector* (pp. 1–22), London, UK: University College London.
- Guo, J., Feng, X., Forbes, J. M., Lei, J., Zhang, J., & Tan, C. (2010). On the relationship between thermosphere density and solar wind parameters during intense geomagnetic storms. *Journal of Geophysical Research*, 115(A12), A12335. <https://doi.org/10.1029/2010JA015971>
- Haines, C., Owens, M. J., Barnard, L., Lockwood, M., & Ruffenach, A. (2019). The variation of geomagnetic storm duration with intensity. *Solar Physics*, 294, 154. <https://doi.org/10.1007/s11207-019-1546-z>
- Happgood, M. (2019). The great storm of May 1921: An exemplar of a dangerous space weather event. *Space Weather*, 17(7), 950–975. <https://doi.org/10.1029/2019SW002195>
- Happgood, M. A. (2011). Toward a scientific understanding of the risk from extreme space weather. *Advances in Space Research*, 47(12), 2059–2072. <https://doi.org/10.1016/j.asr.2010.02.007>
- Hayakawa, H., Ebihara, Y., Cliver, E. W., Hattori, K., Toriumi, S., & Love, J. J. (2019). The extreme space weather event in September 1909. *Monthly Notices of the Royal Astronomical Society*, 484(3), 4083–4099. <https://doi.org/10.1093/mnras/sty3196>
- Hayakawa, H., Ebihara, Y., Pevtsov, A. A., Bhaskar, A., Karachik, N., & Oliveira, D. M. (2020). Intensity and time series of extreme solar-terrestrial storm in 1946 March. *Monthly Notices of the Royal Astronomical Society*, 497(4), 5507–5517. <https://doi.org/10.1093/mnras/staa1508>
- Hayakawa, H., Ebihara, Y., Willis, D. M., Toriumi, S., Iju, T., Hattori, K., et al. (2019). Temporal and spatial evolutions of a large sunspot group and great auroral storms around the Carrington Event in 1859. *Space Weather*, 17(11), 1553–1569. <https://doi.org/10.1029/2019SW002269>
- Hayakawa, H., Ribeiro, P., Vaquero, J. M., Gallego, M. C., Knipp, D. J., Mekhaldi, F., et al. (2020). The extreme space weather event in 1903 October/November: An outburst from the quiet sun. *Astrophysical Journal Letters*, 897(1), L10. <https://doi.org/10.3847/2041-8213/ab6a18>
- Hazard, D. L. (1918). *Results of observations made at the United States Coast and Geodetic Survey magnetic observatory at Cheltenham*. Maryland, 1915 and 1916 (pp. 1–112), Government Printing Office, Washington, DC.
- Hazard, D. L. (1920). Magnetic storm of March 22-23, 1920. *Journal of Geophysical Research*, 25(2), 57–59. <https://doi.org/10.1029/TE025i002p00057>
- Hazard, D. L. (1922a). *Results of observations made at the United States Coast and Geodetic survey magnetic observatory near Honolulu, Hawaii, 1919 and 1920*. (pp. 1–97). Washington, DC: Government Printing Office.
- Hazard, D. L. (1922b). *Results of observations made at the United States Coast and Geodetic Survey magnetic observatory near Tucson, Arizona, 1919 and 1920*. (pp. 1–98). Washington, DC: Government Printing Office.
- Hazard, D. L. (1923). *Results of observations made at the United States Coast and Geodetic Survey magnetic observatory at Vieques, P. R., 1919 and 1920* (pp. 1–100). Washington, DC: Government Printing Office.
- Hewitt, K. (1970). Probabilistic approaches to discrete natural events: A review and theoretical discussion. *Economic Geography*, 46, 332–349. <https://doi.org/10.2307/143148>
- Instituto y Observatorio de Marina. (1893). *Anales del Instituto y Observatorio de Marina de San Fernando, Sección 2, Observaciones Meteorológicas, Magnéticas y Sísmicas, Año 1892* (pp. 1–166). Establecimiento Tipográfica de Don José María Gay Y Bru, San Fernando, Spain.
- Instituto y Observatorio de Marina. (1921). *Anales del Instituto y Observatorio de Marina de San Fernando, Sección 2, Observaciones Meteorológicas, Magnéticas y Sísmicas, Año 1919*. Sección Tipográfica del Observatorio (pp. 1–166), Sección Tipográfica del Observatorio, San Fernando, Spain.
- Jankowski, J., & Sucksdorff, C. (1996). *Guide for Magnetic Measurements and Observatory Practice* (pp. 1–235), Warsaw, Poland: International Association of Geomagnetism and Aeronomy.
- Johnson, N. L., Kotz, S., & Balakrishnan, N. (1995). *Continuous univariate distributions*. New York, NY: John Wiley & Sons.
- Johnston, H. F. (1927). Principal magnetic storms and earthquakes recorded at the Watheroo Magnetic Observatory, July to December, 1926. *Journal of Geophysical Research*, 32(1), 38–40. <https://doi.org/10.1029/TE032i001p00038>
- Johnston, H. F. (1928). Watheroo Magnetic Observatory July, 1928. *Terrestrial Magnetism and Atmospheric Electricity*, 33(4), 259–259. <https://doi.org/10.1029/TE033i004p00259>
- Jonas, S., McCarron, E., & Murtagh, W. (2016). Space weather policy and effects. *Insight*, 19(4), 20–23. <https://doi.org/10.1002/inst.12121>

- Jordanova, V. K., Thorne, R. M., Farrugia, C. J., Dotan, Y., Fennell, J. F., Thomsen, M. F., et al. (2001). Ring current dynamics during the 13–18 July 2000 storm period. *Solar Physics*, *204*(1), 361–375. <https://doi.org/10.1023/A:1014241527043>
- Kakioka Magnetic Observatory. (1959). *Report of the Kakioka magnetic observatory, 1956* (Vol. 26, pp. 1–68), Kakioka, Japan.
- Kamide, Y., Baumjohann, W., Daglis, I. A., Gonzalez, W. D., Grande, M., Joselyn, J. A., et al. (1998). Current understanding of magnetic storms: Storm-substorm relationships. *Journal of Geophysical Research*, *103*(A8), 17705–17728. <https://doi.org/10.1029/98JA01426>
- Kappenman, J. (2012). A perfect storm of planetary proportions. *IEEE Spectrum*, *49*(2), 26–31. <https://doi.org/10.1109/MSPEC.2012.6139230>
- Karinen, A., & Mursula, K. (2005). A new reconstruction of the Dst index for 1932–2002. *Annales Geophysicae*, *23*(2), 475–485. <https://doi.org/10.5194/angeo-23-475-2005>
- Kataoka, R. (2013). Probability of occurrence of extreme magnetic storms. *Space Weather*, *11*(5), 214–218. <https://doi.org/10.1002/swe.20044>
- Katz, R. W., Parlange, M. B., & Naveau, P. (2002). Statistics of extremes in hydrology. *Advances in Water Resources*, *25*(8–12), 1287–1304. [https://doi.org/10.1016/S0309-1708\(02\)00056-8](https://doi.org/10.1016/S0309-1708(02)00056-8)
- Kerridge, D. J. (2001). INTERMAGNET: Worldwide near-real-time geomagnetic observatory data. In *Proceedings of the ESA Space Weather Workshop*. ESTEC, Noordwijk. Retrieved from https://swe.ssa.esa.int/TECEES/spweather/workshops/SPW_W3/PROCEEDINGS_W3/ESTEC_Intermagnet.pdf
- Kilpua, E. K. J., Olsper, N., Grigorievskiy, A., Käpylä, M. J., Tanskanen, E. I., Miyahara, H., et al. (2015). Statistical study of strong and extreme geomagnetic disturbances and solar cycle characteristics. *The Astrophysical Journal*, *806*(2), 1–7. <https://doi.org/10.1088/0004-637X/806/2/272>
- Kilpua, E., Koskinen, H. E. J., & Pulkkinen, T. I. (2017). Coronal mass ejections and their sheath regions in interplanetary space. *Living Reviews in Solar Physics*, *14*(1), 83. <https://doi.org/10.1007/s41116-017-0009-6>
- Klimas, A. J., Valdivia, J. A., Vassiliadis, D., Baker, D. N., Hesse, M., & Takalo, J. (2000). Self-organized criticality in the substorm phenomenon and its relation to localized reconnection in the magnetospheric plasma sheet. *Journal of Geophysical Research*, *105*(A8), 18765–18780. <https://doi.org/10.1029/1999JA000319>
- Knipp, D. J., Ramsay, A. C., Beard, E. D., Boring, A. L., Cade, W. B., Hewins, I. M., et al. (2016). The May 1967 great storm and radio disruption event: Extreme space weather and extraordinary responses. *Space Weather*, *14*(9), 614–633. <https://doi.org/10.1002/2016SW001423>
- Koskinen, H., Eliasson, L., Holback, B., Andersson, L., Eriksson, A., Mälkki, A., et al. (2010). Space Weather and Interactions with Spacecraft. In ESA Technology research program, space environments and effects major Axis (pp. 1–196).
- Kotzé, P. B. (2018). Hermanus Magnetic Observatory: A historical perspective of geomagnetism in southern Africa. *History of Geo- and Space Sciences*, *9*(2), 125–131. <https://doi.org/10.5194/hgss-9-125-2018>
- Lakhina, G. S., & Tsurutani, B. T. (2018). Super geomagnetic storms: Past, present and future. chap. 7. In N. Buzulukova (Ed.), *Extreme space weather: Origins, predictability, and consequences* (pp. 157–185). Elsevier.
- Lanzerotti, L. J. (1992). Comment on “Great magnetic storms” by Tsurutani et al. *Geophysical Research Letters*, *19*(19), 1991–1992. <https://doi.org/10.1029/92GL02238>
- Lefèvre, L., Vennerström, S., Dumbović, M., Vršnak, B., Sudar, D., Arlt, R., et al. (2016). Detailed Analysis of Solar Data Related to Historical Extreme Geomagnetic Storms: 1868 – 2010. *Solar Physics*, *291*, 1483–1531. <https://doi.org/10.1007/s11207-016-0892-3>
- Le, G., Cai, Z., Wang, H., & Zhu, Y. (2012). Solar cycle distribution of great geomagnetic storms. *Astrophysics and Space Science*, *339*, 151–156. <https://doi.org/10.1007/s10509-011-0960-y>
- Lockwood, M., Chambodut, A., Barnard, L. A., Owens, M. J., Clarke, E., & Mendel, V. (2018). A homogeneous aa index: 1. Secular variation. *Journal of Space Weather and Space Climate*, *8*, A53. <https://doi.org/10.1051/swsc/2018038>
- Lockwood, M., Owens, M. J., Barnard, L. A., Scott, C. J., Watt, C. E., & Bentley, S. (2018). Space climate and space weather over the past 400 years: 2. Proxy indicators of geomagnetic storm and substorm occurrence. *Journal of Space Weather and Space Climate*, *8*, A12. <https://doi.org/10.1051/swsc/2017048>
- Loewe, C. A., & Prössl, G. W. (1997). Classification and mean behavior of magnetic storms. *Journal of Geophysical Research*, *102*(A7), 14209–14213. <https://doi.org/10.1029/96JA04020>
- Love, J. J. (2008). Magnetic monitoring of Earth and space. *Physics Today*, *61*(2), 31–37. <https://doi.org/10.1063/1.2883907>
- Love, J. J. (2020). Some experiments in extreme-value statistical modeling of magnetic superstorm intensities. *Space Weather*, *18*(1), e2019SW002255. <https://doi.org/10.1029/2019SW002255>
- Love, J. J., & Chulliat, A. (2013). An international network of magnetic observatories. *Eos, Transactions American Geophysical Union*, *94*(42), 373–374. <https://doi.org/10.1002/2013EO42001>
- Love, J. J., & Finn, C. A. (2011). The USGS Geomagnetism Program and its role in space weather monitoring. *Space Weather*, *9*(7), S07001. <https://doi.org/10.1029/2011SW000684>
- Love, J. J., & Gannon, J. L. (2009). Revised Dst and the epicycles of magnetic disturbance: 1958–2007. *Annales Geophysicae*, *27*, 3101–3131. <https://doi.org/10.5194/angeo-27-3101-2009>
- Love, J. J., Hayakawa, H., & Cliver, E. W. (2019a). On the intensity of the magnetic superstorm of September 1909. *Space Weather*, *17*(1), 37–45. <https://doi.org/10.1029/2018SW002079>
- Love, J. J., Hayakawa, H., & Cliver, E. W. (2019b). Intensity and impact of the New York Railroad superstorm of May 1921. *Space Weather*, *17*(8), 1281–1292. <https://doi.org/10.1029/2019SW002250>
- Love, J. J., Lucas, G. M., Kelbert, A., & Bedrosian, P. A. (2018). Geoelectric Hazard Maps for the Mid-Atlantic United States: 100 Year Extreme Values and the 1989 Magnetic Storm. *Geophysical Research Letters*, *45*(1), 5–14. <https://doi.org/10.1002/2017GL076042>
- Love, J. J., Rigler, E. J., Pulkkinen, A., & Riley, P. (2015). On the lognormality of historical magnetic storm intensity statistics: Implications for extreme-event probabilities. *Geophysical Research Letters*, *42*(16), 6544–6553. <https://doi.org/10.1002/2015GL064842>
- Lucas, G. M., Love, J. J., Kelbert, A., Bedrosian, P. A., & Rigler, E. J. (2020). A 100-year geoelectric hazard analysis for the U.S. high-voltage power grid. *Space Weather*, *18*(2), e2019SW002329. <https://doi.org/10.1002/2019SW002329>
- Lyon, J. G. (2000). The solar wind-magnetosphere-ionosphere system. *Science*, *288*(5473), 1987–1991. <https://doi.org/10.1126/science.288.5473.1987>
- Magnetic Observatory, University of Cape Town. (1944). *Magnetic observations. 1937, 1938, 1939 and 1940*. Pretoria, South Africa: Government Printer.
- Marshall, A. W., & Olkin, I. (2007). *Life distributions: Structure of nonparametric, semiparametric, and parametric families*, Springer series in statistics (pp. 1–782), New York, NY: Springer Science+Business Media.
- Mayaud, P. N. (1980). Derivation, Meaning, and Use of Geomagnetic Indices. Geophysical Monograph 22 (pp. 1–154). Washington, DC: American Geophysical Union). <https://doi.org/10.1029/GM022>

- Menvielle, M., Iyemori, T., Marchaudon, A., & Nosé, M. (2011). Geomagnetic indices. In M. Manda, & M. Korte (Eds.), *Geomagnetic observations and models* (pp. 183–227). Springer.
- Milan, S. E., Hutchinson, J., Boakes, P. d., & Hubert, B. (2009). Influences on the radius of the auroral oval. *Annales Geophysicae*, *27*, 2913–2924. <https://doi.org/10.5194/angeo-27-2913-2009>
- Minamoto, Y. (2013). Availability and Access to Data from Kakioka Magnetic Observatory, Japan. *Data Science Journal*, *12*, G30–G35. <https://doi.org/10.2481/dsj.G-040>
- Mitzenmacher, M. (2004). A brief history of generative models for power law and lognormal distributions. *Internet Mathematics*, *1*(2), 226–251. <https://doi.org/10.1080/15427951.2004.10129088>
- Moos, N. A. F. (1910). *Colaba magnetic data, 1846 to 1905. Part I: Magnetic data and instruments* (pp. 1–263). Bombay, India: Government Central Press.
- Moriña, D., Serra, I., Puig, P., & Corral, Á. (2019). Probability estimation of a Carrington-like geomagnetic storm. *Scientific Reports*, *9*(1), 2393. <https://doi.org/10.1038/s41598-019-38918-8>
- Morley, S. K. (2020). Challenges and opportunities in magnetospheric space weather prediction. *Space Weather*, *18*(3), e2018SW002108. <https://doi.org/10.1029/2018SW002108>
- Mugele, R. A., & Evans, H. D. (1951). Droplet size distribution in sprays. *Industrial & Engineering Chemistry*, *43*(6), 1317–1324. <https://doi.org/10.1021/ie50498a023>
- Mursula, K., Holappa, L., & Karinen, A. (2008). Correct normalization of the Dst index. *Astrophysics and Space Sciences Transactions*, *4*(2), 41–45. <https://doi.org/10.5194/astra-4-41-2008>
- Nagaraja, H. N. (1982). Record values and extreme value distributions. *Journal of Applied Probability*, *19*(1), 233–239. <https://doi.org/10.2307/3213934>
- National Science and Technology Council. (2019). *National space weather strategy and action plan* (pp. 1–13), Executive Office, Washington, DC.
- Nelson, J. H. (1941). Tucson Magnetic Observatory, July to September, 1941. *Terrestrial Magnetism and Atmospheric Electricity*, *46*(4), 475–475. <https://doi.org/10.1029/TE046i004p00475-01>
- Newell, P. T., Sotirelis, T., Liou, K., Meng, C.-I., & Rich, F. J. (2007). A nearly universal solar wind-magnetosphere coupling function inferred from 10 magnetospheric state variables. *Journal of Geophysical Research*, *112*(A1), a. A01206. <https://doi.org/10.1029/2006JA012015>
- Newitt, L. R. (2007). Observatories, automation. In D. Gubbins, & E. Herrero-Bervera (Eds.), *Encyclopedia of geomagnetism and paleomagnetism* (pp. 713–715). Springer.
- Newman, M. (2005). Power laws, Pareto distributions and Zipf's law. *Contemporary Physics*, *46*(5), 323–351. <https://doi.org/10.1080/00107510500052444>
- Ngwira, C. M., Pulkkinen, A., Wilder, F. D., & Crowley, G. (2013). Extended study of extreme geoelectric field event scenarios for geomagnetically induced current applications. *Space Weather*, *11*(3), 121–131. <https://doi.org/10.1002/swe.20021>
- Nikitina, L., Trichtchenko, L., & Boteler, D. H. (2016). Assessment of extreme values in geomagnetic and geoelectric field variations for Canada. *Space Weather*, *14*(7), 481–494. <https://doi.org/10.1002/2016SW001386>
- North American Electric Reliability Corporation. (1990). March 13, 1989 geomagnetic disturbance. In *1989 system disturbances* (pp. 36–60).
- O'Brien, T. P., Fennell, J. F., Roeder, J. L., & Reeves, G. D. (2007). Extreme electron fluxes in the outer zone. *Space Weather*, *5*(1). <https://doi.org/10.1029/2006SW000240>
- Ogg, A. (1946). Hermanus Magnetic Observatory January to March, 1946. *Journal of Geophysical Research*, *51*(2), 298–301. <https://doi.org/10.1029/TE051i002p00298>
- Oliveira, D. M., & Zesta, E. (2019). Satellite orbital drag during magnetic storms. *Space Weather*, *17*(11), 1510–1533. <https://doi.org/10.1029/2019SW002287>
- Oughton, E. J., Skelton, A., Horne, R. B., Thomson, A. W. P., & Gaunt, C. T. (2017). Quantifying the daily economic impact of extreme space weather due to failure in electricity transmission infrastructure. *Space Weather*, *15*(1), 65–83. <https://doi.org/10.1002/2016SW001491>
- Parkinson, W. C. (1921). The magnetic storm of May 13-17, 1921, at Watheroo Observatory, Australia. *Journal of Geophysical Research*, *26*(1-2), 26–28. <https://doi.org/10.1029/TE026i001p00026-02>
- Parkinson, W. C. (1941). Watheroo magnetic observatory, January to March, 1941. *Journal of Geophysical Research*, *46*(2), 260–261. <https://doi.org/10.1029/TE046i002p00260>
- Parkinson, W. C. (1946). Watheroo magnetic observatory January to March, 1946. *Journal of Geophysical Research*, *51*(2), 295–298. <https://doi.org/10.1029/TE051i002p00295>
- Press, W. H., Teukolsky, S. A., Vetterling, W. T., & Flannery, B. P. (1992). *Numerical recipes* (pp. 1–963), Cambridge University Press, Cambridge, UK.
- Pudovkin, M. I., Raspopov, O. M., Leontyev, S. V., & Troitskaya, V. A. (1972). Some peculiarities of the development of the magnetic storm on March, 5-10 1970. *Annales Geophysicae*, *28*(2), 455–463.
- Pulkkinen, A., Bernabeu, E., Eichner, J., Beggan, C., & Thomson, A. W. P. (2012). Generation of 100-year geomagnetically induced current scenarios. *Space Weather*, *10*(4). <https://doi.org/10.1029/2011SW000750>
- Pulkkinen, A., Klimas, A., Vassiliadis, D., Uritsky, V., & Tanskanen, E. (2006). Spatiotemporal scaling properties of the ground geomagnetic field variations. *Journal of Geophysical Research*, *111*(A3), A03305. <https://doi.org/10.1029/2005JA011294>
- Qian, L., & Solomon, S. C. (2012). Thermospheric density: An overview of temporal and spatial variations. *Space Science Reviews*, *168*, 147–173. <https://doi.org/10.1007/s11214-011-9810-z>
- Rasson, J. L., Toh, H., & Yang, D. (2010). The global geomagnetic observatory network. In M. Manda, & M. Korte (Eds.), *Geomagnetic observations and models* (pp. 1–25). Dordrecht, The Netherlands: Springer.
- Ribeiro, P., Vaquero, J. M., Gallego, M. C., & Trigo, R. M. (2016). The first documented space weather event that perturbed the communication networks in Iberia. *Space Weather*, *14*(7), 464–468. <https://doi.org/10.1002/2016SW001424>
- Richardson, I. G., & Cane, H. V. (2012). Solar wind drivers of geomagnetic storms during more than four solar cycles. *Journal of Space Weather and Space Climate*, *2*(A01), A01. <https://doi.org/10.1051/swsc/2012001>
- Riley, P. (2012). On the probability of occurrence of extreme space weather events. *Space Weather*, *10*, aS02012. <https://doi.org/10.1029/2011SW000734>
- Riley, P. (2018). Statistics of extreme space weather events. In N. Buzulukova (Ed.), *Extreme space weather: Origins, predictability, and consequences* (chap. 5, pp. 115–138). Amsterdam, The Netherlands: Elsevier.
- Riley, P., Baker, D., Liu, Y. D., Verronen, P., Singer, H., & Güdel, M. (2018). Extreme space weather events: From cradle to grave. *Space Science Reviews*, *214*(1), 21. <https://doi.org/10.1007/s11214-017-0456-3>

- Riley, P., & Love, J. J. (2017). Extreme geomagnetic storms: Probabilistic forecasts and their uncertainties. *Space Weather*, 15(1), 53–64. <https://doi.org/10.1002/2016SW001470>
- Roe, B. P. (2001). *Probability and statistics in experimental physics, undergraduate texts in contemporary physics* (pp. 1–264). Springer-Verlag, New York, NY.
- Rossi, C. E. (1990). *Failure of electrical power equipment due to solar magnetic disturbances*. Information Notice No. 90-42 (pp. 1–3), U.S. Nuclear Regulatory Commission, Washington, DC.
- Sammis, I., Tang, F., & Zirin, H. (2000). The dependence of large flare occurrence on the magnetic structure of sunspots. *Astrophysical Journal*, 540, 583–587. <https://doi.org/10.1086/309303>
- Schrijver, C. J., Kauristie, K., Aylward, A. D., Denardini, C. M., Gibson, S. E., Glover, A., et al. (2015). Understanding space weather to shield society: A global road map for 2015–2025 commissioned by COSPAR and ILWS. *Advances in Space Research*, 55(12), 2745–2807. <https://doi.org/10.1016/j.asr.2015.03.023>
- Schröder, W., & Wiederkehr, K.-H. (2000). A history of the early recording of geomagnetic variations. *Journal of Atmospheric and Solar-Terrestrial Physics*, 62(5), 323–334. [https://doi.org/10.1016/S1364-6826\(99\)00100-5](https://doi.org/10.1016/S1364-6826(99)00100-5)
- Schulte in den Bäumen, H., Moran, D., Lenzen, M., Cairns, I., & Steenge, A. (2014). How severe space weather can disrupt global supply chains. *Natural Hazards and Earth System Sciences*, 14(10), 2749–2759. <https://doi.org/10.5194/nhess-14-2749-2014>
- Silbergleit, V. M. (1997). On the occurrence of the largest geomagnetic storms per solar cycle. *Journal of Atmospheric and Solar-Terrestrial Physics*, 59(2), 259–262. [https://doi.org/10.1016/S1364-6826\(96\)00002-8](https://doi.org/10.1016/S1364-6826(96)00002-8)
- SILSO World Data Center. (1902–2016). *The international sunspot number, international sunspot number monthly Bulletin and online catalog*.
- Silverman, S. M. (1995). Low latitude auroras: the storm of 25 September 1909. *Journal of Atmospheric and Terrestrial Physics*, 57(6), 673–685. [https://doi.org/10.1016/0021-9169\(94\)e0012-c](https://doi.org/10.1016/0021-9169(94)e0012-c)
- Silverman, S. M., & Cliver, E. W. (2001). Low-latitude auroras: the magnetic storm of 14–15 May 1921. *Journal of Atmospheric and Solar-Terrestrial Physics*, 63(5), 523–535. [https://doi.org/10.1016/S1364-6826\(00\)00174-7](https://doi.org/10.1016/S1364-6826(00)00174-7)
- Siscoe, G., Crooker, N. U., & Clauer, C. R. (2006). *Dst* of the Carrington storm of 1859. *Advances in Space Research*, 38(2), 173–179. <https://doi.org/10.1016/j.asr.2005.02.102>
- Siscoe, G. L. (1976a). On the statistics of the largest geomagnetic storms per solar cycle. *Journal of Geophysical Research*, 81(25), 4782–4784. <https://doi.org/10.1029/JA081i025p04782>
- Siscoe, G. L. (1976b). A *Dst* contribution to the equatorward shift of the aurora. *Planetary and Space Science*, 27(7), 997–1000. [https://doi.org/10.1016/0032-0633\(79\)90029-1](https://doi.org/10.1016/0032-0633(79)90029-1)
- Solow, A. R., & Beet, A. R. (2004). A note on the statistics of the largest geomagnetic storms per solar cycle. *Journal of Atmospheric and Solar-Terrestrial Physics*, 66(18), 1731–1732. <https://doi.org/10.1016/j.jastp.2003.12.010>
- Sornette, D. (2006). *Critical phenomena in natural sciences: Chaos, fractals, selforganization and disorder: Concepts and tools* (pp. 1–528). Springer-Verlag, Berlin, Germany.
- Spanier, J., & Oldham, K. B. (1987). *An atlas of functions* (pp. 1–700). Hemisphere Publishing, Harper & Row, New York, NY.
- Steinskog, D. J., Tjøstheim, D. B., & Kvamstø, N. G. (2007). A cautionary note on the use of the Kolmogorov-Smirnov test for normality. *Monthly Weather Review*, 135(3), 1151–1157. <https://doi.org/10.1175/MWR3326.1>
- Sugiura, M. (1964). Hourly values of equatorial *Dst* for the IGY. *Annals of the International Geophysical Year*, 35(9–45).
- Sugiura, M., & Kamei, T. (1991). Equatorial *Dst* Index 1957–1986, IAGA Bull. (Vol. 40). International Service of Geomagnetic Indices Publications Office, Saint-Maur-des-Fosses, France.
- Superintendent of the U.S. Naval Observatory. (1892). The magnetic storm of February 13–14, 1892. *Nature*, 45(1169), 493. <https://doi.org/10.1038/045493a0>
- Thomsen, M. F. (2004). Why *Kp* is such a good measure of magnetospheric convection. *Space Weather*, 2(11), a. 004. <https://doi.org/10.1029/2004SW000089>
- Thomson, A. W. P. (2007). Geomagnetic hazards. In D. Gubbins, & E. Herrero-Bervera (Eds.), *Encyclopedia of geomagnetism and paleomagnetism* (pp. 316–319). Dordrecht, The Netherlands: Springer.
- Tsiftis, T., & De la Luz, V. (2018). Extreme value analysis of solar flare events. *Space Weather*, 16(12), 1984–1996. <https://doi.org/10.1029/2018SW001958>
- Tsubouchi, K., & Omura, Y. (2007). Long-term occurrence probabilities of intense geomagnetic storm events. *Space Weather*, 5, a. S12003. <https://doi.org/10.1029/2007SW000329>
- Tsurutani, B. T., Gonzalez, W. D., Gonzalez, A. L. C., Guarnieri, F. L., Gopalswamy, N., Grande, M., et al. (2006). Corotating solar wind streams and recurrent geomagnetic activity: A review. *Journal of Geophysical Research*, 111 A07S01. <https://doi.org/10.1029/2005JA011273>
- Tsurutani, B. T., Gonzalez, W. D., Lakhina, G. S., & Alex, S. (2003). The extreme magnetic storm of 1–2 September 1859. *Journal of Geophysical Research*, 108(A7), 1268. <https://doi.org/10.1029/2002JA009504>
- Tukey, J. W. (1977). *Exploratory data analysis* (pp. 1–714). Reading, MA: Addison-Wesley.
- Turcotte, D. L. (1999). Self-organized criticality. *Report on Progress in Physics*, 62(10), 1377–1429. <https://doi.org/10.1088/0034-4885/62/10/201>
- Uritsky, V. M., & Pudovkin, M. I. (1998). Low frequency 1/f-like fluctuations of the AE-index as a possible manifestation of self-organized criticality in the magnetosphere. *Annales Geophysicae*, 16(12), 1580–1588. <https://doi.org/10.1007/s00585-998-1580-x>
- Various (1957). *Annals of the International Geophysical Year. parts IV–V* (Vol. IV, pp. 207–329). Pergamon Press, London, UK.
- Vassiliadis, D., Klimas, A. J., Baker, D. N., & Roberts, D. A. (1995). A description of the solar wind-magnetosphere coupling based on non-linear filters. *Journal of Geophysical Research*, 100(A3), 3495–3512. <https://doi.org/10.1029/94JA02725>
- Vasyliūnas, V. M. (2011). The largest imaginable magnetic storm. *Journal of Atmospheric and Solar-Terrestrial Physics*, 73(11–12), 1444–1446. <https://doi.org/10.1016/j.jastp.2010.05.012>
- Vennerstrom, S., Lefevre, L., Dumbović, M., Crosby, N., Malandraki, O., Patsou, I., et al. (2016). Extreme geomagnetic storms - 1868 - 2010. *Solar Physics*, 291(5), 1447–1481. <https://doi.org/10.1007/s11207-016-0897-y>
- Veselovsky, I. S., Dmitriev, A. V., & Suvorova, A. V. (2010). Algebra and statistics of the solar wind. *Cosmic Research*, 48(2), 113–128. <https://doi.org/10.1134/S0010952510020012>
- von Storch, H. (1995). Misuses of statistical analysis in climate research. In H. von Storch, & A. Navarra (Eds.), *Analysis of climate variability: Applications and statistical techniques*. (pp. 11–25). New York NY: Springer-Verlag.
- Walshaw, D. (2013). Generalized extreme value distribution. In A. H. El-Shaarawi, & W. W. Piegorsch (Eds.), *Encyclopedia of environmental statistics*. New York, NY: John Wiley & Sons. <https://doi.org/10.1002/9780470057339.vae062.pub2>
- Wanliss, J. (2005). Fractal properties of SYM-H during quiet and active times. *Journal of Geophysical Research*, 110, A03202. <https://doi.org/10.1029/2004JA010544>

- Watari, S., Kunitake, M., & Watanabe, T. (2001). The Bastille day (14 JULY 2000) event in historical large Sun-Earth connection events. *Solar Physics*, 204(1), 425–438. <https://doi.org/10.1023/A:1014273227639>
- Webb, D. F., Cliver, E. W., Crooker, N. U., St Cyr, O. C., & Thompson, B. J. (2000). Relationship of halo coronal mass ejections, magnetic clouds, and magnetic storms. *Journal of Geophysical Research*, 105(A4), 7491–7508. <https://doi.org/10.1029/1999JA000275>
- Webb, D. F., & Howard, R. A. (1994). The solar cycle variation of coronal mass ejections and the solar wind mass flux. *Journal of Geophysical Research*, 99(A3), 4201–4220. <https://doi.org/10.1029/93JA02742>
- Webb, H. D. (1969). Solar flares and magnetic storm of May 21 to 28, 1967. *Journal of Geophysical Research*, 74(7), 1880–1882. <https://doi.org/10.1029/JA074i007p01880>
- Weigel, R. S., & Baker, D. N. (2003). Probability distribution invariance of 1-minute auroral-zone geomagnetic field fluctuations. *Geophysical Research Letters*, 30(23), 2193. <https://doi.org/10.1029/2003GL018470>
- Welling, D. T. (2019). Magnetohydrodynamic models of B and their use in GIC estimates. In J. L. Gannon, A. Swidinsky, & Z. Xu (Eds.), *Geomagnetically induced currents from the sun to the power grid. Geophysical Monograph 244* (chap. 3, pp. 43–65). Washington, DC: American Geophysical Union. <https://doi.org/10.1002/9781119434412.ch3>
- White, R. F. (1941). Tucson Magnetic Observatory, January to March, 1941. *Journal of Geophysical Research*, 46(2), 257–258. <https://doi.org/10.1029/TE046i002p00257>
- Wik, M., Pirjola, R., Lundstedt, H., Viljanen, A., Wintoft, P., & Pulkkinen, A. (2009). Space weather events in July 1982 and October 2003 and the effects of geomagnetically induced currents on Swedish technical systems. *Annales Geophysicae*, 27, 1775–1787. <https://doi.org/10.5194/angeo-27-1775-2009>
- Wilks, D. S. (2019). *Statistical Methods in the Atmospheric Sciences* (Vols. 1–818). The Netherlands: Elsevier, Amsterdam.
- Willis, D. M., Stevens, P. R., & Crothers, S. R. (1997). Statistics of the largest geomagnetic storms per solar cycle (1844–1993). *Annales Geophysicae*, 15(6), 719–728. <https://doi.org/10.1007/s00585-997-0719-5>
- Woodroffe, J. R., Morley, S. K., Jordanova, V. K., Henderson, M. G., Cowee, M. M., & Gjerloev, J. G. (2016). The latitudinal variation of geoelectromagnetic disturbances during large ($Dst \leq -100$ nT) geomagnetic storms. *Space Weather*, 14(9), 668–681. <https://doi.org/10.1002/2016SW001376>
- World Data Center for Geomagnetism, Kyoto, Nosé, M., Iyemori, T., Sugiura, M., & Kamei, T. (2015). *Geomagnetic Dst index*. <https://doi.org/10.17593/14515-74000>
- Wu, C.-C., Liou, K., Lepping, R. P., Huttig, L., Plunkett, S., Howard, R. A., & Socker, D. (2016). The first super geomagnetic storm of solar cycle 24: “The St. Patrick’s day event (17 March 2015)”. *Earth Planets and Space*, 68. <https://doi.org/10.1186/s40623-016-0525-y>
- Yermolaev, Y. I., Lodkina, I. G., Nikolaeva, N. S., & Yermolaev, M. Y. (2013). Occurrence rate of extreme magnetic storms. *Journal of Geophysical Research: Space Physics*, 118(8), 4760–4765. <https://doi.org/10.1002/jgra.50467>
- Yokoyama, N., Kamide, Y., & Miyaoka, H. (1998). The size of the auroral belt during magnetic storms. *Annales Geophysicae*, 16(5), 566–573. <https://doi.org/10.1007/s00585-998-0566-z>
- Zhang, J., Liemohn, M. W., Kozyra, J. U., Lynch, B. J., & Zurbuchen, T. H. (2004). A statistical study of the geoeffectiveness of magnetic clouds during high solar activity years. *Journal of Geophysical Research*, 109(A9), A09, 101. <https://doi.org/10.1029/2004JA010410>